Cancer Cell

Article

The pre-existing T cell landscape determines the response to bispecific T cell engagers in multiple myeloma patients

Graphical abstract

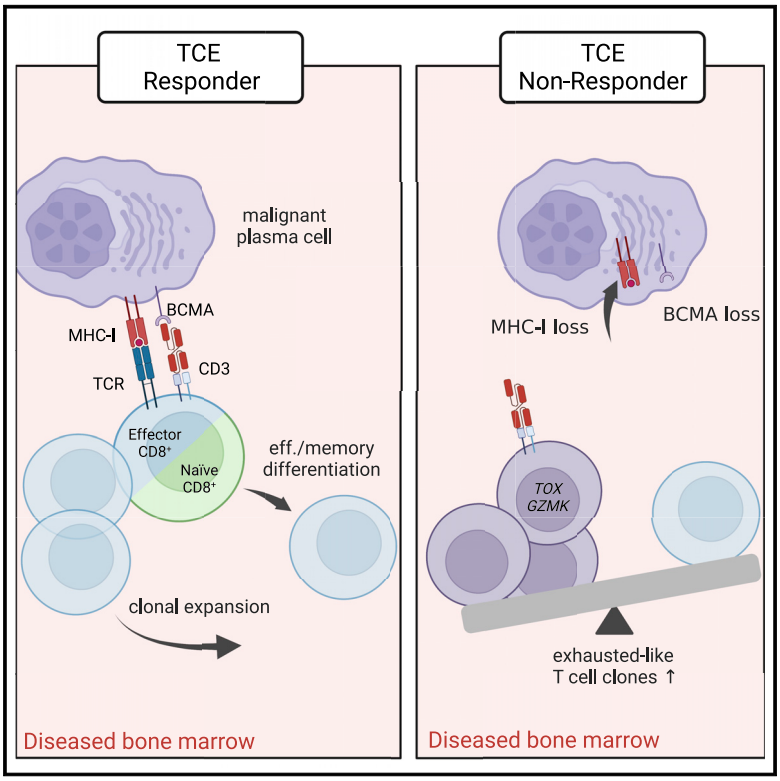

Highlights

- Single-cell TCR tracing identifies conserved T cell responses to TCEs in humans
- Clonal expansion of effector CD8$^+$ T cells is an immunological driver of TCE therapy
- Naive T cells require additional MHC class I signal and differentiate upon TCE activation
- The abundance of exhausted CD8$^+$ clones predicts response failure in multiple myeloma

Authors

Mirco J. Friedrich, Paola Neri, Niklas Kehl, ..., Carsten Müller-Tidow, Marc-Steffen Raab, Nizar J. Bahlis

Correspondence

mfriedri@broadinstitute.org (M.J.F.), marc.raab@med.uni-heidelberg.de (M.-S.R.), nbahlis@ucalgary.ca (N.J.B.)

In brief

Bispecific T cell engagers (TCEs) have shown promise in the treatment of various cancers, but their mode of action in humans is elusive. Providing new insight into immunological mechanisms, Friedrich et al. identify how T cells in multiple myeloma patients respond to TCEs according to their cell state and link inter-individual differences in the immune repertoire to clinical response.

Friedrich et al., 2023, Cancer Cell *41*, 711–725
April 10, 2023
https://doi.org/10.1016/j.ccell.2023.02.008

CellPress

Cancer Cell

CellPress
OPEN ACCESS

Article

The pre-existing T cell landscape determines the response to bispecific T cell engagers in multiple myeloma patients

Mirco J. Friedrich,[1,2,14,17,*] Paola Neri,[3,4,14] Niklas Kehl,[5,6,15] Julius Michel,[5,6,15] Simon Steiger,[7,8] Michael Kilian,[5,6] Noémie Leblay,[4] Ranjan Maity,[4] Roman Sankowski,[9] Holly Lee,[3,4] Elie Barakat,[4] Sungwoo Ahn,[4] Niels Weinhold,[1] Karsten Rippe,[7] Lukas Bunse,[5,6] Michael Platten,[5,6,10,11,12] Hartmut Goldschmidt,[1,11] Carsten Müller-Tidow,[1,11] Marc-Steffen Raab,[1,13,16,*] and Nizar J. Bahlis[3,4,16,*]

[1]Department of Hematology, Oncology and Rheumatology, Heidelberg University Hospital, Heidelberg, Germany
[2]Broad Institute of MIT and Harvard, Cambridge, MA 02142, USA
[3]Arnie Charbonneau Cancer Research Institute, University of Calgary, Calgary, Canada
[4]Tom Baker Cancer Center, Department of Hematology and Oncology, Calgary, Canada
[5]Clinical Cooperation Unit Neuroimmunology and Brain Tumor Immunology, German Cancer Research Center (DKFZ), Heidelberg, Germany
[6]Department of Neurology, MCTN, Medical Faculty Mannheim, Heidelberg University, Mannheim, Germany
[7]Division of Chromatin Networks, BioQuant Center & German Cancer Research Center (DKFZ), Heidelberg, Germany
[8]Faculty of Biosciences, Heidelberg University, Heidelberg, Germany
[9]Department of Neuropathology, Freiburg University Hospital, Freiburg, Germany
[10]Helmholtz Institute of Translational Oncology (HI-TRON), Mainz, Germany
[11]National Center for Tumor Diseases (NCT), Heidelberg, Germany
[12]DKFZ Hector Cancer Institute at the University Medical Center Mannheim, Mannheim Germany
[13]Clinical Cooperation Unit Molecular Hematology/Oncology, German Cancer Research Center (DKFZ), Heidelberg, Germany
[14]These authors contributed equally
[15]These authors contributed equally
[16]These authors contributed equally
[17]Lead contact
*Correspondence: mfriedri@broadinstitute.org (M.J.F.), marc.raab@med.uni-heidelberg.de (M.-S.R.), nbahlis@ucalgary.ca (N.J.B.)
https://doi.org/10.1016/j.ccell.2023.02.008

SUMMARY

Bispecific T cell engagers (TCEs) have shown promise in the treatment of various cancers, but the immunological mechanism and molecular determinants of primary and acquired resistance to TCEs remain poorly understood. Here, we identify conserved behaviors of bone marrow-residing T cells in multiple myeloma patients undergoing BCMAxCD3 TCE therapy. We show that the immune repertoire reacts to TCE therapy with cell state-dependent clonal expansion and find evidence supporting the coupling of tumor recognition via major histocompatibility complex class I (MHC class I), exhaustion, and clinical response. We find the abundance of exhausted-like $CD8^+$ T cell clones to be associated with clinical response failure, and we describe loss of target epitope and MHC class I as tumor-intrinsic adaptations to TCEs. These findings advance our understanding of the *in vivo* mechanism of TCE treatment in humans and provide the rationale for predictive immune-monitoring and conditioning of the immune repertoire to guide future immunotherapy in hematological malignancies.

INTRODUCTION

Immunotherapy has transformed the treatment landscape of many cancers in recent years. Despite substantial success, however, durable responses with immunotherapy are usually achieved in only a subset of patients.[1,2] To improve this outcome, we need a better understanding of the molecular mechanisms of immunotherapy, and we need to identify predictive indicators for treatment response. Single-cell characterization of pre- and on-treatment biopsies has provided important insights into the patterns of T cell expansion and the mechanisms underlying this process. To date, however, these studies are limited to either easy-to-biopsy cancer types (such as melanoma), small numbers of patients, or focusing exclusively on immune cell composition.[3–5]

T cell infiltrates in human tumors are heterogeneous in terms of functional state and T cell receptor (TCR)-mediated tumor cell recognition.[6,7] In hematologic malignancies, such as multiple myeloma (MM), deciphering the determinants of response to immunotherapy is further complicated by a highly perturbed and heterogeneous immune repertoire that differs in cell-type composition, gene expression, clonality, and functional

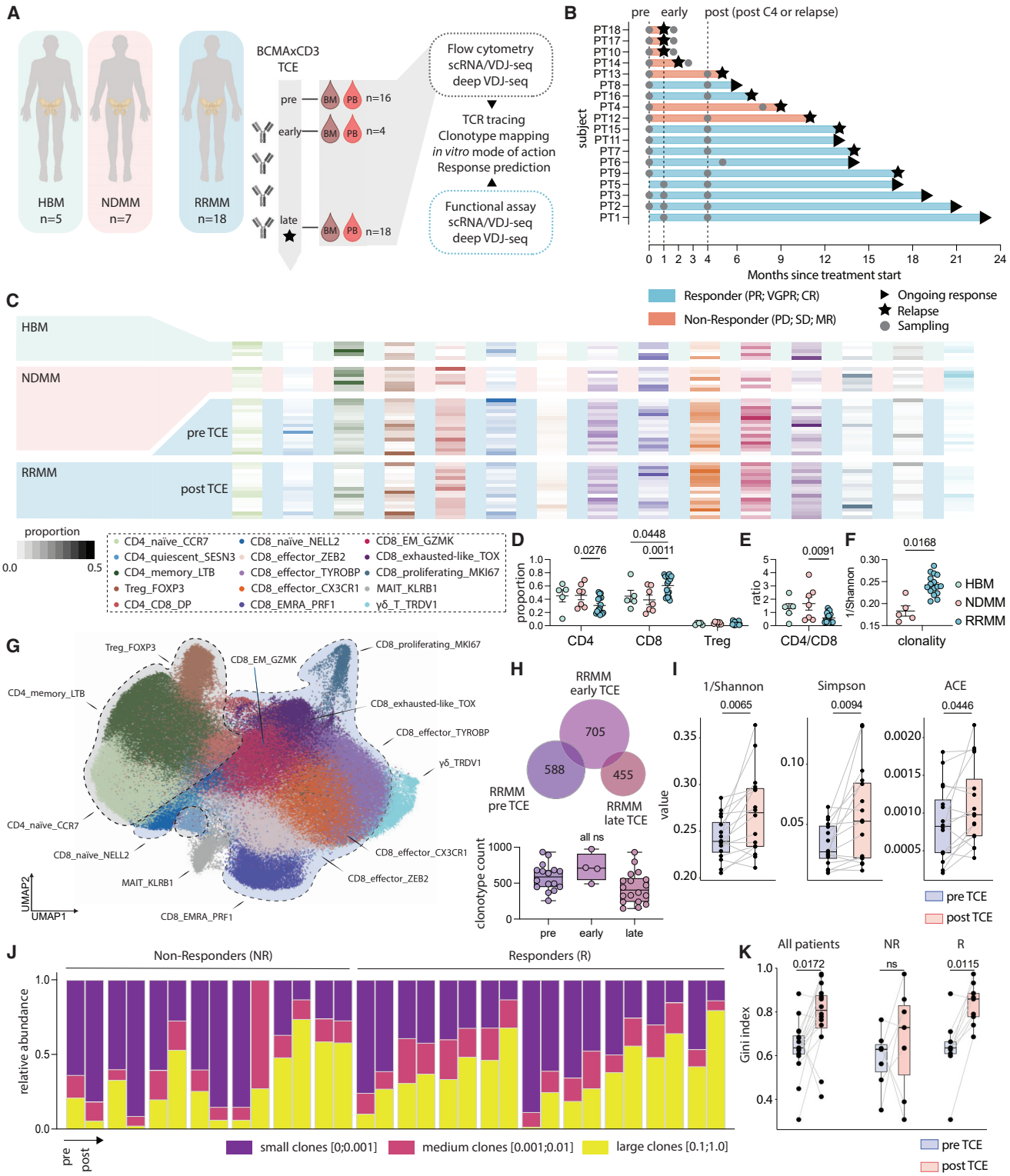

Figure 1. The bone marrow-associated T cell repertoire responds to CD3-targeting immunotherapy with clonal expansion

(A) Design of the study in bone marrow and peripheral blood-derived samples of healthy bone marrow (BM) donors, newly diagnosed multiple myeloma (NDMM) patients, and RRMM patients receiving TCE therapy.

(B) Swimmer plot indicating RRMM subjects' response to treatment over time and sampling time points.

(legend continued on next page)

properties.[8,9] Immune repertoire plasticity is further influenced by tumor load, disease stage, and therapy.[10–13] Finally, the individual patient's bone marrow niche is heterogeneous with respect to cellular composition and the ability to control tumor growth.[14–16] These factors make it challenging to identify and monitor immune cells driving anti-tumoral response against hematological cancers.

In several cancers, such as melanoma or lung cancer, clonal expansion of T cells drives treatment response to immune checkpoint blockade (ICB).[5,17,18] It is presently controversial whether circulating T cells with various levels of exhaustion markers contribute to therapeutic efficacy or merely have predictive value in immunotherapy.[18,19] In murine models, T cells with high expression of exhaustion markers appear refractory to reinvigoration by ICB. Nevertheless, the frequency of dysfunctional T cells expressing high levels of PD-1 has been shown to correlate with clinical response to anti-PD-1 therapy in NSCLC patients.[20,21] Other mechanisms of resistance may involve immune suppression by tumor-associated myeloid cells, regulatory T cells (Tregs), or the expression of inhibitory immune checkpoints, as well as downregulation of tumor-associated antigens resulting in tumor escape.[22,23]

Bispecific T cell engagers (TCEs) are designed to overcome some of these challenges associated with targeting tumor-associated antigens (TAAs) by linking two antibody fragments that recognize distinct epitopes on the TAAs and on the T cell surface. By bridging the T cell and tumor cell, TCEs are believed to trigger a cascade of events that lead to T cell activation and subsequent tumor cell lysis. In MM, TCEs achieve high clinical response rates.[24–28] However, resistance appears to invariably occur, and some patients fail to respond to TCE therapy, even when TCE target antigens are highly expressed.[29] Loss of target antigen has recently been shown to be associated with acquired resistance to TCEs,[30] but it is unknown if additional immunological mechanisms of primary and acquired resistance exist. Moreover, given the occurrence of primary response failures in some patients, it is critical to identify predictive indicators of TCE response to guide treatment strategies. To address these gaps, we have performed a comprehensive longitudinal profiling of the bone marrow T cell repertoire and its response to the perturbance created by TCE treatment and integrated additional experimental data using primary cells isolated from human patients to delineate the molecular mode of action of TCEs. Our results identify conserved behaviors of bone marrow-residing $CD4^+$ and $CD8^+$ T cells in MM patients undergoing TCE therapy and establish T cell state and tumor recognition as prerequisites of clonal T cell expansion and clinical response in non-solid tumors.

RESULTS

The bone marrow-associated T cell repertoire responds to CD3-targeting immunotherapy with clonal expansion

The currently most often used T cell-engaging agents are bispecific antibodies targeting an epitope on the tumor cell surface as well as the CD3 receptor on T cells, but it is not clear how the bone marrow-resident and peripheral immune system communicates and responds to these antibodies in humans. To understand the molecular mechanisms of TCE response in MM, we first sought to characterize the response of the bone marrow-resident and peripheral T cell repertoire to TCE therapy.

We employed MM as a model disease because it is closely associated with the bone marrow immune microenvironment and serial bone marrow biopsies are available from patients on experimental single-agent BCMAxCD3 bispecific antibody treatment.[28] We analyzed the transcriptome and TCR repertoire of bone marrow-associated immune cells from a total of 30 healthy bone marrow (HBM) donors (N = 5), newly diagnosed MM (NDMM) patients (N = 7), and relapsed/refractory MM (RRMM) (N = 18) patients receiving BCMAxCD3 bispecific antibody monotherapy (Figure 1A; Tables S1 and S2). Publicly available HBM and NDMM scRNA-seq datasets were re-analyzed within this study using the same quality control pipeline as in-house samples and then integrated into the final dataset.[8] Longitudinal iliac crest site-matched bone marrow biopsies and peripheral blood draws were performed on TCE-receiving patients to allow

(C) Bone marrow immune repertoire composition gradients. Each line represents one biological sample (healthy donor or patient). Proportion of indicated cell types relative to total bone marrow immune repertoire is represented by the color gradient. Samples from RRMM patients receiving TCE therapy are ordered according to treatment cycle.

(D and E) Cellular composition changes in multiple myeloma. (D) Proportion of $CD4^+$, $CD8^+$, and regulatory (Treg) T cells per condition in dataset subset to T cells. (E) Evaluation of CD4/CD8 ratio in dataset subset to T cells per condition. Mean ± SEM shown. Statistical significance was determined by one-way ANOVA and Bonferroni's multiple comparison test.

(F) Comparison of TCR clonality (1/Shannon index) at diagnosis between NDMM and RRMM with available scVDJ-seq data. Mean ± SEM shown. N = 21 evaluable patients, mean ± SEM and unpaired t test results shown.

(G) Uniform Manifold Approximation and Projection (UMAP) map of T cell subset displaying a total of 248,478 T cells annotated in 4 groups and 15 clusters and marked by color code.

(H) Longitudinal assessment of TCR clonotypes in the bone marrow of TCE therapy-receiving patients. Top: bubble plot visualization of median clonotype count per individual at the indicated time points. Bottom: quantification of median clonotype count at the indicated time points. N = 16 evaluable patients. Quantification was performed following downsampling to n = 1,000 cells. Boxplot showing median ± SEM, whiskers indicate full range of values. Statistical significance was determined by one-way ANOVA and Bonferroni's multiple comparison test.

(I) TCR repertoire diversity metrics in RRMM patients receiving TCE therapy at the indicated time points. N = 16 evaluable patients. Boxplot showing median ± SEM, whiskers indicate 10–90 percentile. Paired t test results shown.

(J) Bar chart indicating clonal space homeostasis within each TCE patient sample analyzed at the indicated time points. Relative abundance of clones shown. Frequency cut points: small = [0;0.001], medium = [0.001;0.01], large = [0.01;1].

(K) Gini index of TCR clonal space in RRMM patients receiving TCE therapy at the indicated time points. N = 16 evaluable patients. Each patient time point was downsampled to the minimum number of T cells captured in either of the paired patient datasets. Boxplot showing median ± SEM, whiskers indicate 10–90 percentile. Statistical significance was determined by repeated measures one-way ANOVA and Bonferroni's multiple comparison test. See also Figures S1–S4 and Tables S1 and S2.

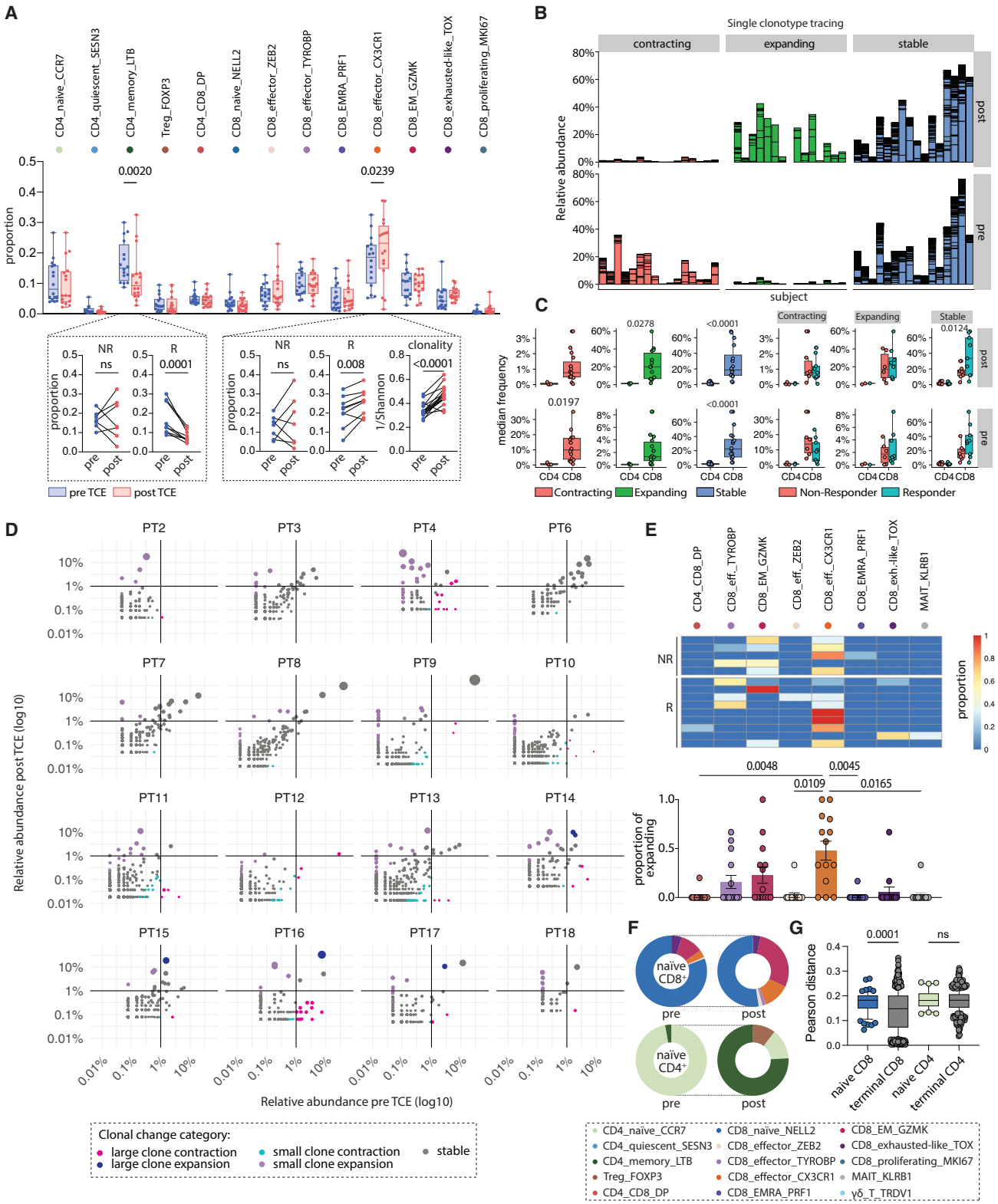

Figure 2. TCE response is driven by CD8⁺ effector cells

(A) Top: comparison of transcriptionally defined T cell cluster proportions in the bone marrow pre- and post-TCE therapy. N = 16 evaluable patients. Bottom: comparison of T cell cluster proportion pre- and post-TCE therapy split by clinical response. N = 9 clinical responders (R), N = 7 clinical non-responders (NR).

(legend continued on next page)

for analyses of the immune repertoire at the time points during therapy (“pre” = prior to treatment initiation; “early” = post cycle 1; “late” = post-cycle 4 or at relapse; Figure 1B). By tracing T cell clones over time using their TCR amino acid sequence as an individual barcode, we further integrated longitudinal data with global and individual repertoire-level analyses. After stringent quality control and filtering, we obtained a total of 325,571 bone marrow-associated immune cells from 5 HBM, 7 NDMM, and 18 RRMM donors (Figures S1A and S1B). T cells were further grouped into 63,374 distinct clonotypes by matching both α and β chain pairs and matched with peripheral blood bulk TCRβ-sequencing of patients, allowing us to track clonal lineages and measure overlap and dynamics of single clones in bone marrow and blood.

We generated an overview of global changes in cell composition of healthy and diseased bone marrow spanning MM evolution as well as treatment with TCEs (Figures 1C and S1C–S1E). Recent studies demonstrated an early accumulation of Tregs, followed by loss of $CD8^+$ memory populations as early as the smoldering myeloma stage, suggesting a loss of immunosurveillance in the bone marrow niche preceding MM progression.[31,32] In our cohort, RRMM patients did not demonstrate increased Treg numbers, but increased counts of $CD8^+$ T cells compared with NDMM patients (Figure 1D). Taken together with a reduced abundance of $CD4^+$ T cells in the diseased bone marrow, this results in a decreased $CD4^+/CD8^+$ ratio in RRMM patients, a known key cellular composition defect in MM (Figure 1E).[33,34] Notably, this increase in absolute $CD8^+$ cell counts was underlain by an increase in clonality in RRMM compared with NDMM patients (Figures 1F, S1F, and S1G). To understand the effects of TCE therapy on the MM bone marrow-associated T cell landscape, we proceeded to characterize a total of 248,478 T cells from all 30 samples annotated in four groups ($CD8^+$, $CD4^+$, $\gamma\delta$ T, and MAIT; Figures 1G and S2A–S2C). We defined 5 functional $CD4^+$ and 8 functional $CD8^+$ T cell clusters based on canonical patterns of marker expression across conditions, spanning all canonical trajectories of naive T cells following effector-memory fates, as well as Treg and proliferating $CD8^+$ cells (Figures 1G and S3A–S3C). It was recently shown that human memory $CD8^+$ T cells are a heterogeneous population consisting of Granzyme K (*GZMK*)$^+$ and *GZMK*$^-$ subsets.[35] *GZMK*$^+$ memory T cells co-express markers of T cell exhaustion and are committed to give rise to T cells with an exhausted phenotype. Interestingly, we found a population of *GZMK*$^+$ $CD8^+$ T cells in the bone marrow of all analyzed RRMM patients, albeit at variable frequency. Compared with other $CD8^+$ cells in our dataset, this cluster had significantly reduced expression of cytotoxicity markers (*PRF1*, *GZMB*) and TCF-1 (*TCF7*) as well as co-expression of the exhaustion markers *PDCD1* and *LAG3* with the fate regulator *TOX* (Figures 1G and S4A–S4C).

We next analyzed the bone marrow TCR repertoire of 16 TCE-receiving patients with available paired data pre- and on-treatment and observed a significant increase in global clonality over the course of treatment, while the absolute number of clonotypes did not differ significantly across sampling time points (Figures 1H, 1I, and S2C). Notably, using the Gini index as a measure of inequality in clonotype size across samples, we found that the index significantly increases on therapy, reflecting the emergence of more highly expanded clones in response to TCE exposure (Figures 1J and 1K). Importantly, clinical responder patients demonstrated significant clonal expansion in response to TCEs, which is in line with previous studies investigating response patterns to ICB,[4,5] where absolute clonotype expansion correlated with clinical response (Figure 1K).

TCE response is driven by $CD8^+$ effector cells

We next sought to delineate which transcriptionally defined T cell subsets undergo clonal expansion in response to therapy and therefore compared the proportion of each T cell cluster before and after TCE exposure. We found that CD4_memory_LTB T cells significantly declined in proportion on treatment. By contrast, CD8_effector_CX3CR1 significantly increased on treatment. Notably, the proportional increase of CD8_effector_CX3CR1 cells was consistently found in clinical responders and underlain by an increase in clone size, whereas clinical non-responders appear to exhibit mixed changes (Figure 2A).

To identify single clones that significantly change in response to therapy, we applied a bootstrapping approach stratified to the number of cells for each time point, accounting for sampling error of the identified TCR sequences. With this approach, we were able to calculate empirical p values for each TCR clone, identify

Comparison of TCR clonality (1/Shannon index) pre- and post-TCE therapy of CD8_effector_CX3CR1 cluster shown. Statistical significance was determined by repeated measures two-way ANOVA and Bonferroni’s multiple comparison test.

(B–D) Longitudinal tracing of single TCR clones in TCE therapy-receiving patients. Significant clonotype dynamics were determined by a bootstrapping approach stratified to number of cells at each time point followed by Benjamini-Hochberg correction for multiple testing. All clones derived from N = 16 patients with adjusted p values >0.05 shown. (B) Staggered bar chart indicating cumulative abundance of traceable single TCR clones with significant clonotype dynamics on TCE therapy. (C) Comparison of $CD4^+$ and $CD8^+$ clones (left) and all clones derived from clinical non-responders and responders (right) within clonal change categories. Boxplot showing median ± SEM, whiskers indicate 10–90 percentile. Statistical significance was determined by one-way ANOVA and Bonferroni’s multiple comparison test. (D) Scatterplot indicating traceable single TCR clones and their corresponding clonal change on TCE therapy for each evaluated patient. T cell count in each clone is indicated by dot size.

(E) Top: heatmap of significantly expanding TCR clonotype counts and corresponding transcriptionally defined T cell cluster in the bone marrow of clinical responder (R) and non-responder (NR) patients. Bottom: comparison of T cell cluster proportions in significantly expanding TCR clonotypes. N = 16 evaluable patients. Mean ± SEM shown. Statistical significance was determined by one-way ANOVA and Tukey’s multiple comparison test.

(F) Donut plots indicating phenotype composition of initially majority-naive (>50%) $CD4^+/CD8^+$ clones (pre-therapy) that were traced between therapy time points.

(G) Pearson distance of gene expression profiles in TCR clones on TCE treatment. The Pearson distance of gene expression profiles ((1- Pearson correlation)/2) over the course of TCE treatment (pre- vs. post-treatment) was assessed for each TCR clone. Clones that were initially composed of >50% naive $CD4^+/CD8^+$ cells were compared with clones that were initially composed of >50% terminally differentiated $CD4^+/CD8^+$ cells. Boxplot showing median ± SEM, whiskers indicate 10–90 percentile. Statistical significance was determined by one-way ANOVA and Bonferroni’s multiple comparison test. See also Figures S5–S7.

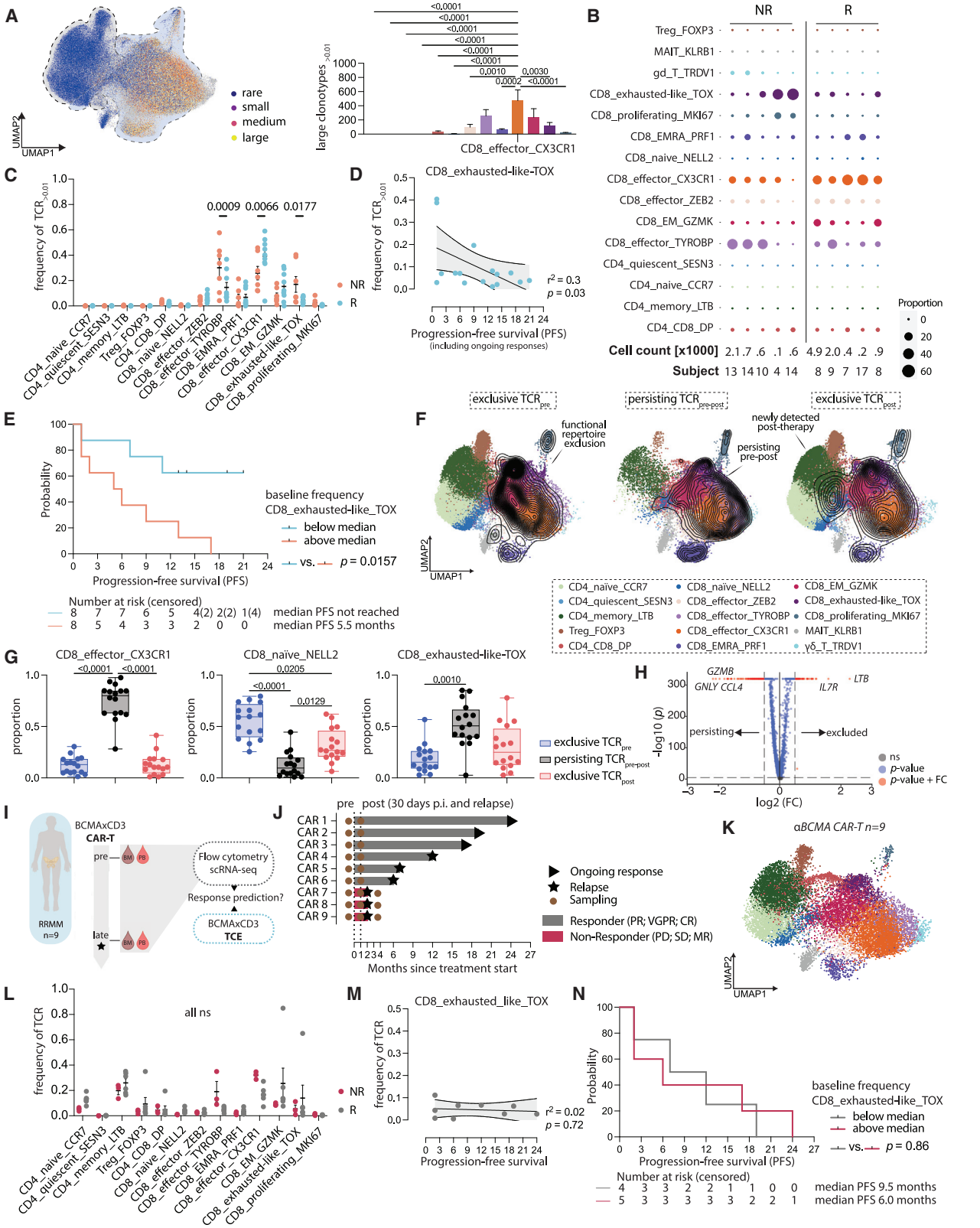

Figure 3. The abundance of clonal exhausted-like T cells predicts response to TCE therapy

(A) Left: UMAP map of subclustered T cells overlaid by clone size of clonotypes found in the TCE cohort. Relative abundance of clones in distinct sizes as indicated by the color-coded legend. Frequency cut points: rare = [0;0.0001], small = [0.0001;0.001], medium = [0.001;0.01], large = [0.01;1]. Right: comparison of

(legend continued on next page)

clones with significant fold change between time points, and define categories of clonal changes (Figures 2B–2D and S5). We then characterized the transcriptional phenotype associated with each of these categories and compared differential changes between them. We identified T cell clones that significantly expanded or contracted on therapy, although the frequency of most clones remained constant over time, suggesting that a generally stable bone marrow TCR repertoire responds to TCE exposure with clonal changes in some, but not all, T cell subsets (Figures 2B and 2C). Clonotypes undergoing empirically significant clonal changes were enriched for $CD8^+$ T cells. Specifically, and reflective of their proportional change on therapy (Figure 2A), single TCR clones demonstrating relevant clone expansion were significantly enriched for CD8_effector_CX3CR1 T cells (Figures 2D and 2E).

The observed increase of effector $CD8^+$ cells upon TCE therapy might be further explained by homing of differentiated cells from the periphery. However, the extent to which the peripheral immune system contributes novel effector T cells to local cancer-affected compartments such as the bone marrow remains ill-understood. In addition, both hematological malignancies and immunotherapies perturb this communication. We therefore performed deep VDJ-seq on matched bone marrow and peripheral blood samples of TCE patients and found an increase in the fraction of clonotypes overlapping between bone marrow and peripheral blood post-therapy, but not pre-therapy (Figures S6, S7A, and S7B). Furthermore, most clonotypes that we found to be expanded upon treatment in the bone marrow could also be detected in peripheral blood and vice versa, but not all contracted clonotypes were found in both compartments, likely falling below the limit of detection or binomial sampling probability upon contraction (Figures S7C and S7D). Although this experimental approach cannot discriminate if this is a result of active homing of T cells or increased inter-compartmental communication facilitated by TCE effects, these findings are consistent with the prior notion in solid oncology that T cells expanding in the periphery could serve as a pool of tumor-homing T cells.[17]

We hypothesized that, in addition to clonal expansion or homing of pre-existing clones, the increased abundance of effector $CD8^+$ T cells in TCE-treated patients might be the result of an induced phenotypic shift of naive T cells to effector states. As a result of clonal expansion and differentiation, however, TCR clonotypes co-exist at different states at the same time, resulting in transcriptionally heterogeneous, but related populations sharing the same TCR. Therefore, to test our hypothesis, we mapped the phenotype composition of all pre-existing majority-naive (>50%) T cell clones (n = 95) over time (Figures 2F and 2G). We found that after therapy, initially naive $CD8^+$ T clones were found in effector and memory clusters, while initially naive T cells were enriched for memory and Treg states (Figure 2F). Transcriptional change between cells of the same clonotype can indicate differentiation or phenotype diversification of that clonotype. For each T cell clone, we therefore computed the Pearson distances between the transcriptional profiles before and after therapy. We observed a significantly increased transcriptome distance over time in $CD8^+$ T cell clones that were majority-naive before treatment start, when compared with terminally differentiated $CD8^+$ T cell clones (Figures 2G and S7E). This likely results in the assignment of progeny cells of initially naive T cell clones to multiple transcriptional clusters post-therapy (Figure 2F). Conversely, we did not detect significant differences in the

expanded clonotypes between CD8_effector_CX3CR1 and other transcriptionally defined T cell clusters. N = 16 evaluable patients. Mean ± SEM shown. Statistical significance was determined by one-way ANOVA and Bonferroni's multiple comparison test.

(B) Dot plot of top 10 clonal TCRs by clone size in all RRMM patients before treatment with TCEs. All T cell clonotypes from clinical responders (R), (n = 9) and non-responders (NR) (n = 7) were pooled for analysis. Phenotype distribution of each clonotype into specified cell subsets is marked by color code. Clone size and subject of each derived TCR clone is indicated.

(C) Comparison of pre-existent frequency of each transcriptionally defined T cell cluster in the clonal bone marrow T cell repertoire (>0.01) of clinical R (n = 9) and NR (n = 7) to anti-BCMA TCE therapy. Mean ± SEM shown. Statistical significance was determined by two-way ANOVA and Bonferroni's multiple comparison test.

(D) Correlation between pre-existent abundance of CD8_exhausted-like_TOX clonal T cells in the bone marrow and duration of response in TCE-treated patients (N = 16). Patients with ongoing responses were included in the analysis using the respective last PFS follow-up time point. Linear regression shown.

(E) Kaplan-Meier survival analysis shown in TCE-treated patients (N = 16) stratified by pre-existent abundance of CD8_exhausted-like_TOX clonal T cells in the bone marrow of anti-BCMA TCE-treated patients (N = 16). Progression-free survival (PFS) shown. Log rank (Mantel-Cox) test was used for comparison of survival curves. All censored patients (n = 4) demonstrated ongoing response before the end of the study.

(F) UMAP map of subclustered T cells overlaid by a density gradient indicating location and abundance of highly clonal TCRs (frequency > 0.01): exclusive TCR_{pre}, exclusive clonotypes pre-therapy; persisting $TCR_{pre\text{-}post}$, persisting clonotypes found throughout therapy; exclusive TCR_{post}, exclusive clonotypes post-therapy.

(G) Proportion of time point-exclusive and persisting clones in the bone marrow with CD8_effector_CX3CR1 (top) and CD8_naive_NELL2 (bottom) phenotype. Boxplot showing median ± SEM, whiskers indicate full range of values. Statistical significance was determined by one-way ANOVA and Bonferroni's multiple comparison test.

(H) Volcano plot depicting differential gene expression between TCR clones that are persisting on-therapy (persisting) and TCR clones that are exclusively found pre-therapy (excluded). p values adjusted by Benjamini-Hochberg correction for multiple testing are shown.

(I) Design of the study in bone marrow and peripheral blood-derived samples of RRMM patients receiving anti-BCMA CAR-T cell therapy.

(J) Swimmer plot indicating RRMM subjects' response to treatment over time and sampling time points.

(K) UMAP map of subclustered T cells. A total of 14,673 T cells from N = 9 patients were reference mapped to *in vivo* dataset (Figures 1–4), annotated in 15 clusters, and marked by color code.

(L) Comparison of pre-existent clonotype frequency for each transcriptionally defined T cell cluster in the bone marrow of clinical R (n = 6) and NR (n = 3) to anti-BCMA CAR-T cell therapy. Mean ± SEM shown. Statistical significance was determined by two-way ANOVA and Bonferroni's multiple comparison test.

(M) Correlation between pre-existent abundance of CD8_exhausted-like_TOX T cells in the bone marrow and duration of response in anti-BCMA CAR-T cell-treated patients (n = 9). Linear regression shown.

(N) Kaplan-Meier survival analysis shown in TCE-treated patients (N = 16) stratified by pre-existent abundance of CD8_exhausted-like_TOX T cells in the bone marrow of anti-BCMA CAR-T cell-treated patients (N = 9). PFS shown. Log rank (Mantel-Cox) test was used for comparison of survival curves. See also Figure S8.

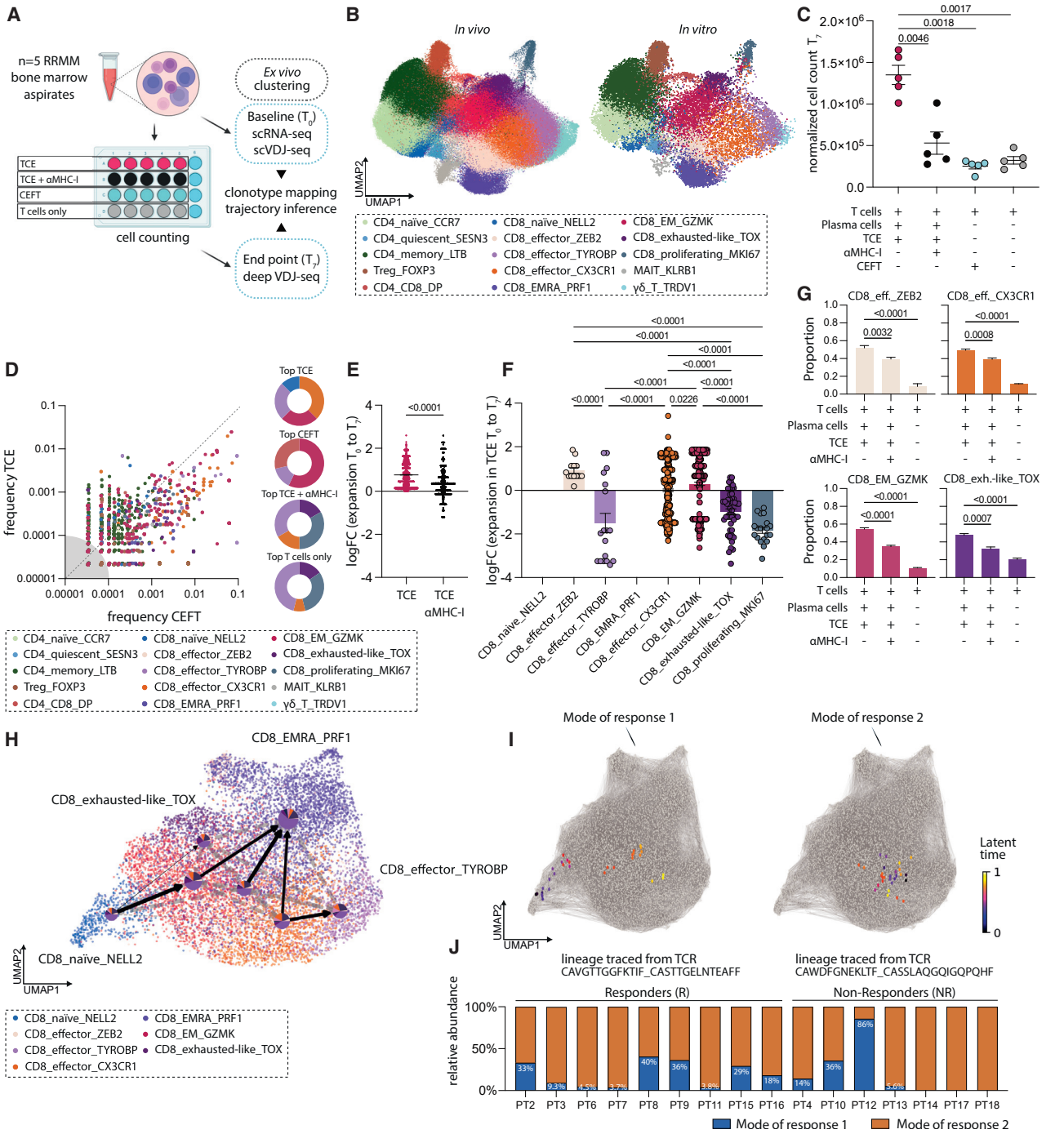

Figure 4. Activation of naive T cells by TCEs requires MHC class I interaction

(A) Experimental overview.

(B) UMAP map of subclustered T cells. A total of 25,312 T cells were reference mapped to the *in vivo* dataset (Figures 1–3), annotated in 15 clusters, and marked by color code.

(C) Cell counts at T_7 normalized to T_0 input cell count. Primary human bone marrow-derived T cells and autologous malignant plasma cells isolated from N = 5 RRMM patients. Mean ± SEM shown. Statistical significance was determined by repeated measures one-way ANOVA and Bonferroni's multiple comparison test.

(D–G) Assessment of differential clonotype expansion between experimental conditions. The frequencies of all TCE-reactive clones in each experimental condition after downsampling to the minimum of cells detected in all conditions were matched to the T_0 frequency of each clone as baseline to compute condition-dependent clonal expansion. Each clonotype was then assigned its baseline phenotype from T_0 transcriptional profiling.

(D) Left: clonotype frequencies of persisting T cell clonotypes from pre- to post-treatment. Cell subsets are indicated by the color-coded legend. Right: donut plots highlighting composition of top 10 expanding clones in response to TCEs, viral peptide library (CEFT), TCE + MHC class I blockade (TCE+αMHC-I) or T cells only control. Cell subsets are indicated by the color-coded legend.

(legend continued on next page)

Pearson distances of initially naive compared with terminally differentiated CD4$^+$ T cell clones.

The abundance of exhausted-like T cell clones is associated with clinical response failure

TCE therapies in MM are currently being investigated in experimental clinical trials, and one BCMAxCD3 bispecific antibody was recently approved for treatment in RRMM by both the Federal Drug Administration and European Medical Agencies.[36–46] So far, no predictive markers of response to TCE therapy have been proposed. Our previous data suggest that an effective TCE response by T cells is dependent on clonal expansion of CD8 effector cells, which together represent the largest clones in our TCE-treated patient cohort (Figure 3A). We therefore hypothesized that a bone marrow T cell landscape dominated by large TCE-receptive T cell clones of the CD8_effector_CX3CR1 phenotype facilitates clinical response, whereas the preponderance of exhausted T cell clones might characterize a bone marrow immune repertoire that is unable to generate sufficient TCE-sensitive T cells and consequently fails to respond to TCEs. Indeed, when performing a meta-analysis of the full RNA/TCR-seq dataset by detaching clonotype information from the individual and integrating the clonality and corresponding phenotype of all evaluated TCRs before treatment, we found that of the top T cell clones in clinical responders, most were enriched for effector states. By contrast, clones derived from non-responder patients were predominantly assigned to the CD8_exhausted-like_TOX cluster before therapy initiation (Figures 3B and S8A).

GZMK$^+$ CD8$^+$ exhausted T cells in NDMM and in older populations have been shown to be associated with rapid disease progression in NDMM and inflammaging, respectively.[47,48] Pre-existing exhausted-like CD8$^+$ T cells contributed to the clonal TCR repertoire of non-responder patients (Figure 3B). Moreover, the proportion of pre-existing exhausted-like CD8$^+$ clones before therapy start was significantly increased in non-responder vs. responder patients. Conversely, the frequency of clonotypes assigned to the CD8_effector_CX3CR1 and CD8_effector_TYROBP clusters was significantly decreased in non-responder vs. responder patients (Figure 3C). The frequency of CD8_exhausted_like_TOX clonotypes was further correlated with progression-free survival in our study cohort (Figures 3D and 3E). Taken together, these data reveal the association of pre-existing T cell exhaustion and clonal expansion capacity with clinical response to TCEs.

As T cell exhaustion is characterized by the progressive loss of T cell function and can culminate in the physical deletion of the responding cells, we evaluated whether pre-existent exhausted-like T cells are cleared by chronic TCE exposure. To assess this, we generated a high-dimensional map that integrates phenotype, clonotype, and compartment dynamics of all TCE-treated patients across non-inferred treatment time points (Figures 3F and 3G). We found that most large CD8_effector_CX3CR1 clones were persisting throughout therapy, in line with their pronounced clonal expansion. In contrast, naive clones were exclusively enriched before and on-therapy, suggesting clonotype loss of pre-existent naive clones as well as detection of novel clones from peripheral blood. Alternatively, naive clones tend to be very small in clone size and therefore more infrequent to detect. Interestingly, a large fraction of CD8_exhausted-like_TOX clonotypes were still detected throughout treatment, although clonal expansion of these clones in response to TCEs was minimal (Figures 3G and 2E). In line with these results, differential gene expression analysis of persisting compared with excluded clones revealed markers of cytotoxicity (*GZMB*, *GNLY*) as well as *CCL4* to be enriched in persisting clones, while excluded clones exhibited increased expression of *IL7R* and *LTB*, which are consistent with a memory-like phenotype (Figures 3H and S8B).

To assess if the abundance of pre-existing exhausted-like CD8$^+$ T cell clones is associated with response to other BCMA-targeted immunotherapies, we performed scRNA-seq on bone marrow-resident T cells of nine RRMM patients receiving anti-BCMA CAR-T cell therapy (Figures 3I and 3J). We reference mapped these data to our BCMAxCD3-TCE *in vivo* clustering to allow for identical definitions of transcriptional clusters (Figure 3K), but we did not find any prognostically relevant association of exhausted-like CD8$^+$ T cells in these patients (Figures 3L–3N). This suggests that our prediction marker is specific to active immunotherapies, such as bispecific TCEs.

Activation of CD8$^+$ T cells by TCEs is amplified by MHC class I:TCR co-signaling

Current TCE designs target the T cell surface glycoprotein CD3 epsilon chain. Response to TCEs is thought to be independent of tumor recognition and T cell state. However, we hypothesized that the pronounced clonal expansion and effector differentiation we observed to be induced by TCEs *in vivo* likely require additional canonical T cell activation signals.

To decipher the immunological mode of action of TCEs, we performed an *in vitro* bone marrow co-culture of primary human bone marrow-derived T cells and autologous malignant plasma cells isolated from RRMM patients treated with functional BCMAxCD3 TCEs (Figures 4A and S9A). CD138$^+$ malignant plasma cells and CD3$^+$ T cells from bone marrow aspirates were isolated by fluorescence-activated cell sorting and co-cultured for 7 days in the presence of functional BCMAxCD3

(E) Clonal expansion of identical TCR clones in response to TCE ± MHC class I blockade from T_0 to T_7. Each dot represents a TCR clone detected in both conditions. Mean logFC ± SEM and paired t test results shown.
(F) Clonal expansion of indicated T cell subsets in response to TCE treatment according to phenotype. Each dot represents a TCR clone detected under the TCE conditions. Mean ± SEM shown. Statistical significance was determined by one-way ANOVA and Bonferroni's multiple comparison test.
(G) Relative abundance of cells in identical TCR clones in response to TCE ± MHC class I blockade or T cells only control. Mean ± SEM shown. Statistical significance was determined by one-way ANOVA and Dunnett's multiple comparison test. Cell subsets color coded as above.
(H) Aggregation of cell-individual fate maps into a cluster-level fate map using a partition-based graph abstraction with directed edges as computed by CellRank scVelo algorithm. Terminal states indicated.
(I) Lineage tracing of representative TCE-reactive TCR clones following computed trajectories on UMAP from (H).
(J) Relative abundance of TCR clones following mode of response 1 (naive-to-effector trajectory) or mode of response 2 (differentiated effector + clonal expansion) in response to TCE treatment. Data for n = 16 evaluable patients shown. See also Figures S9–S11.

TCEs. A viral epitope library (CEFT) encompassing 27 major histocompatibility complex class I (MHC class I)-presented peptides derived from *Clostridium tetani*, Epstein-Barr virus (EBV/HHV-4), human cytomegalovirus (CMV/HHV-5), and influenza A was used to distinguish virus-reactive TCRs. We included an established antibody to block interaction with MHC class I molecules and therefore malignant plasma cell recognition by $CD8^+$ T cells.[19] We thereby hoped to address if TCE-induced expansion and differentiation is co-opted in clones at the time of MM disease progression or acquired due to simultaneous TCE binding and antigen recognition. To allow single-cell readout of the assay, we performed combined scRNA/VDJ-seq at baseline (T_0) followed by bulk TCR-seq at the endpoint (T_7 = 7 days) to detect clonotypes post-assay and link their single-clone expansion in each condition to their pre-assay phenotype by using the highly variable CDR3 amino acid sequence as a unique identifier of each T cell clone (Figures 4A and S9B–S9D).

A total of 25,312 T cells were reference-mapped to the patient *in vivo* dataset (Figure 1G), and cells were assigned to the identical 15 functional T cell clusters to allow translational analysis (Figure 4B). As expected, we observed considerable expansion of T cells when co-cultured with malignant plasma cells and BCMAxCD3 TCEs. Cell counts at T_7 normalized to the T_0 baseline further revealed that clonal expansion was significantly reduced by MHC class I blockade (Figure 4C). We next matched the frequencies of all TCE-reactive clones in each experimental condition after downsampling to the minimum of cells detected in all conditions to the T_0 frequency of each clone as baseline to compute condition-dependent clonal expansion. By discriminating TCE-induced expansion from expansion triggered by the viral epitope library and correcting for unspecific baseline expansion, we defined TCE-reactive [log2FC (E_{TCE}-E_{CEFT}-$E_{T\ cells\ only}$) > 1] and virus-reactive [log2FC (E_{CEFT}-E_{TCE}-$E_{T\ cells\ only}$) > 1] TCRs (Figures 4D and 4E). Each clonotype was then assigned its baseline phenotype from T_0 transcriptional profiling. In line with the *in vivo* data, we found that the top 10% of TCE-responsive clonotypes demonstrated a phenotype within the cytotoxic-effector axis, whereas virus-reactive TCRs were mainly enriched for effector memory $CD8^+$ T cells (Figure 4D). Notably, the expansion of TCE-reactive TCRs was significantly reduced by MHC class I blockade, reproducing the decrease in global T cell count in the assay and suggestive of the need for some TCE-reactive T cell subsets to receive a second activating signal via MHC class I:TCR recognition (Figure 4E).

We further found significant differences in the magnitude of TCE-induced expansion in the $CD8^+$ compartment. Specifically, CD8_effector_ZEB2 and CD8_effector_CX3CR1 T cells demonstrated more pronounced TCE-induced clonal expansion than other $CD8^+$ transcriptional clusters, while we observed contraction of CD8_exhausted-like-TOX T cells upon TCE treatment, which was in line with our *in vivo* findings (Figure 4F). Particularly, MHC class I blockade was effective in reducing clonal expansion in all effector cell subsets, including CD8_effector_CX3CR1 T cells, which we found to drive response *in vivo* (Figure 4G). Interestingly, we could not detect any initially naive $CD8^+$ T cell clones in the MHC class I blockade condition, suggesting that MHC class I-mediated signaling might only be required for those clones that are in a naive state, and that the expansion of T cells we observed in the MHC class I blockade condition is due to clones that are already of the effector phenotype (Figure S9E).

Our assay allows for the detection and tracing of virtually all single T cells that make up a given T cell clonotype in each experimental condition. However, transcriptional information of T cells post-assay was not available and would likely be not fully reflective of T cell biology due to the *in vitro* design of the assay. We therefore sought to infer conserved patterns of response to TCEs using fate mapping.

Current methods to infer trajectories from scRNA-seq data are largely limited to datasets of embryonic development because they require an *a priori* knowledge of developmental direction. To apply these methods for our data, we considered tissue-resident T cells as mostly terminally differentiated. We employed CellRank for single-cell fate mapping and adapted this method for the combined scRNA/VDJ-seq data.[49] With this approach, we inferred the trajectories of TCE-responsive T cells and determined if responsive clones are fate determined or if they exhibit phenotype plasticity that would enable state changes upon TCE exposure. We found that the projected velocities of $CD8^+$ T cells mostly converge to effector/memory states as well as states with a high expression of the dysfunctional gene module signature (Figures 3H, 3I, and S10A–S10C). We next inferred pseudotime along with the initial and terminal states probabilities and identified five cellular macrostates. (Figures S10D and S10E). By employing a modified STEMNET approach, which was initially designed to define the multilineage potential of stem cells, we arranged all T cells according to fate probabilities toward these macrostates.[50] Importantly, CD8_exhausted-like_TOX and CD8_EM_GZMK cells (as identified by the shared transcriptional definition of both (*in vivo*/*in vitro*) datasets) showed almost-exclusive commitment to the CD8_exhausted-like_TOX macrostate, whereas other cells displayed higher heterogeneity (Figure S10E). The top driver genes that defined the CD8_exhausted-like_TOX macrostates in latent time along individual trajectories included the induced transcription of *BTG1*, which was recently shown to be a key factor of T cell quiescence, as well as *SRGN* and the proapoptotic *PMAIP1* gene (Figure S10F).[51]

By single-clone lineage tracing of experimentally validated TCE-responsive T cells, we found two principal modes of TCE response (MoR) on a cellular level (Figures 4I and 4J). First, T cell clones in an initially naive state followed an effector-memory trajectory in line with our findings described in Figure 2, with progeny ultimately found in the $CD8^+$ effector macrostates (MoR 1). Second, T cell clones that were already committed to an effector state at baseline remained in this transcriptional state over latent time (MoR 2). However, these clones displayed pronounced clonal expansion in line with our *in vivo* observations (Figures 2A and 2E). We next quantified the proportion of both MoR for each of the patients studied in our cohort. In line with our previous data, the proportion of cells likely to follow MoR 2 (i.e., clonal expansion without state change of effector $CD8^+$ cells) appeared to outweigh the proportion of cells likely to follow MoR (i.e., naive $CD8^+$ cells undergoing effector differentiation as first response to TCEs) in most patients (Figure 4J). However, as the MoR composition significantly varied between individuals, we have not detected a statistically significant association with clinical response.

Based on these results, we propose that the immunological mode of action of TCE therapy is dependent on the current state of a given T cell. This initial T cell state predisposes the observed distinct degrees of clonal expansion and exhaustion upon TCE exposure. Furthermore, TCE mode of action involves effector differentiation without marked clonal expansion of a limited amount of previously naive T cells, which may be dependent on MHC class I:TCR co-stimulatory signaling.

We propose that the abundance of clonal exhausted-like $CD8^+$ T cell clones in the bone marrow of TCE-receiving patients indicates a higher probability of relapse. Because we found that MHC class I interaction with tumor cells amplified overall T cell response to TCEs *in vitro* by functional recruitment and priming of naive T cell clones, we hypothesized that loss of MHC class I might be a tumor-intrinsic mechanism of acquired resistance in addition to the previously described loss of target epitope expression. To test this, we performed cell-cell interaction analyses in all malignant plasma cells isolated from patients receiving therapy (Figure S11A). We found significant interactions of malignant plasma cells with immune cells via *HLA-C* on therapy (Figure S11B). To quantify the association between a given time point and the expression of ligand and receptor genes on MM cells, we utilized a random forest classifier, a well-established machine learning technique. Based on their importance value for the classification, we identified more MHC class I (*HLA-E*, *HLA-C*) and class II genes (*CD74*) as well as the transcript of the TCE target BCMA (*TNFRSF17*) as relevant plasma cell surface proteins that are regulated in response to TCE treatment (Figures S11C and S11D). We confirmed that loss of BCMA or MHC class I surface expression on malignant plasma cells occurred in some clinical non-responder patients at relapse by flow cytometry (Figures S11D–S11F).

Taken together, these findings demonstrate two modes of action of bispecific TCE treatment in multiple myeloma: the preferential expansion of specific transcriptionally defined T cell clones upon stimulation as well as differentiation and MHC class I-dependent priming of naive T cells. Correspondingly, we describe the loss of MHC receptor molecules as a potential mechanism of TCE-mediated tumor immune escape beyond loss the target antigen.[52] Using this mechanism, malignant cells might escape the additional immune pressure of MHC class I-dependent T cell responses.

DISCUSSION

Advancing cancer immunotherapies requires a more refined understanding of their molecular mechanisms and the pathways that give rise to resistance to these treatments. Such information will not only inform the development of modified immunotherapies but also provide guidance for future treatment strategies. Here, we examined the impact of TCEs on MM patients by performing a longitudinal interrogation of T cells in the peripheral blood and bone marrow of MM patients, coupled with analysis of expanded TCR clonotypes. From these data, we observed that response to TCEs in MM largely results from and is determined by the clonal expansion of a repertoire of pre-existing T cell clones. Our study provides a resource of the diseased and perturbed human T cell repertoire and its response to immunotherapy. We present a map of a highly plastic bone marrow immune landscape that is associated with significant potential for T cell expansion and links the unexpectedly high response of adaptive immunotherapy in multi-refractory hematological malignancies to repertoire fitness. By demonstrating the mechanism of TCE treatment in humans as well as specific mechanisms of immune evasion, we provide the rationale for predictive immune monitoring and conditioning of the immune repertoire to guide future immunotherapy approaches.

Even though TCE therapy was administered in an ongoing phase I clinical trial (NCT03269136), we were able to confirm that early T cell expansion detected in our study led to ongoing responses up to 22 months. In melanoma, peripheral T cell expansion occurring within 3 weeks of starting ICB treatment correlates with improved clinical response to ICB 6 months later.[18] Because we observed a clinical response beyond cycle 4 of TCE therapy, and an initial T cell response was already observed after 30 days, T cell expansion may also be associated with a clinical benefit in MM. Using recently published unbiased trajectory inference methods, we observed that $CD8^+$ T cells showed continuous progression along two specific trajectories after TCE treatment.[49] Most clones showed early effector function but eventually reached a terminal memory or dysfunctional state. Interestingly, $CD4^+$ cells did not contribute significantly to the observed clonal expansion but are likely also supporting secondary TCE responses and have been shown to be vital in maintaining robust antitumor immunity.[53,54] However, most of the $CD4^+$ T cell clones we studied in our dataset were not clonally expanding in response to TCEs. Importantly, none of the hyperexpanded clonotypes in responder patients emerged from exhausted-like $CD8^+$ or $CD4^+$ T cells. This is in striking contrast to non-responders, where hyperexpanded clonotypes post TCEs derived from T cells were fixed in an exhausted-like state. These findings mirror the recent observation in the transplantable Vk*MYC MM animal model, where large disease burden and T cell exhaustion were found to be associated with impaired immunotherapy response.[55]

Our data furthermore suggest molecular targets whose modulation may be synergistic with TCEs. We show that naive $CD8^+$ T cell clones represent an alternative route of TCE-induced immune response. These cells can be further stimulated by allowing MHC class I:TCR interactions.[51] Prior priming of T cells with tumor-associated antigens or intensive immunogenic cell death might therefore sensitize tumors to TCEs. Proteasome inhibitors, such as bortezomib or carfilzomib, have recently been proposed to induce immunogenic cell death but are not considered prime combination partners for TCEs.[56,57] These data could therefore inform future trial designs of TCEs in MM. Similarly, we observed potentially immune-preventing interactions with T cells in patients, including loss of the TCE target antigen BCMA and, surprisingly, loss of genes of the MHC class I and II complex. These findings merit further research into acquired resistance mechanisms in larger cohorts. Overall, our data suggest that induction of MHC class I in tumor cells, e.g., in irradiated extramedullary disease, could be of therapeutic benefit.[58]

A limitation of this and other translational studies investigating dynamics of the TCR repertoire is the longitudinal

detection of only a limited number of T cells with each sampling and the corresponding binomial sampling uncertainty. We aimed to address this by (1) profiling several thousand T cells that passed quality control in our patient samples, (2) application of a bootstrapping approach accounting for sampling error of the identified TCR sequences to identify significant clonal contractions and expansions of the TCR repertoire, and (3) supplementing scVDJ-seq data with deep VDJ-seq of matched bone marrow and peripheral blood samples pre- and on-therapy, when possible. Statistical methods cannot account for sampling error without knowledge of the ground truth within the highly diverse TCR repertoire. Previous studies assumed that the highly non-uniform abundance of TCR clonotypes could best be modeled using a Zipf distribution, which might enable more complete assessments of changes in rare clonotypes.[59] However, by limiting assessment to highly frequent clonotypes in this study, we are confident that we could identify empirically significant clonal dynamics and gain valuable insight into longitudinal changes of the disease-perturbed TCR repertoire. Nevertheless, profiling the full human TCR repertoire in several compartments including transcriptional information therefore remains challenging. Novel high-throughput single-cell sequencing technologies might, however, facilitate these approaches in the future.[60]

STAR★METHODS

Detailed methods are provided in the online version of this paper and include the following:

- KEY RESOURCES TABLE
- RESOURCE AVAILABILITY
  - Lead contact
  - Materials availability
  - Data and code availability
- EXPERIMENTAL MODEL AND SUBJECT DETAILS
  - Human patients
- METHOD DETAILS
  - Processing of human bone marrow samples
  - Processing of human peripheral blood samples
  - Single-cell RNA sequencing and data preprocessing
  - Single-cell transcriptomic analyses
  - Analysis of bone marrow immune cells for cell cell interaction analyses
  - Integration of TCE patient datasets and timepoints
  - RNA velocity analysis of the *in vitro* data
  - Individual clonotype dynamics
  - Reference-based mapping of CAR-T cell-treated patient data to *in vivo* dataset and analysis
  - T cell dysfunction score
  - T cell cytotoxicity score
  - Cell-cell interaction analysis of human bone marrow-associated immune cells
  - Deep TCRB sequencing
  - Functional TCE testing in *in vitro* bone marrow cultures
  - Reference-based mapping of *in vitro* data to *in vivo* dataset and analysis
  - Data visualization
- QUANTIFICATION AND STATISTICAL ANALYSIS

SUPPLEMENTAL INFORMATION

Supplemental information can be found online at https://doi.org/10.1016/j.ccell.2023.02.008.

ACKNOWLEDGMENTS

We thank Rhiannon K. Macrae for careful editing and proofreading of this manuscript. We thank Anja Baumann, Stefanie Jung, and Sandra Bauer for their technical support. We thank the Clinical Myeloma Registry and Biobank at Heidelberg University Hospital that is funded through the Dietmar Hopp Foundation. We are grateful to the DKFZ Genomics and Proteomics and Omics IT and Data Management core facilities for their technical support. This study was supported by the Federal Ministry of Education and Research (BMBF) and the Ministry of Science Baden-Württemberg within the framework of the Excellence Strategy of the Federal and State Governments of Germany (to M.J.F.; Project-ID ExU 6.1.12) and Deutsche José Carreras Leukämie-Stiftung (DJCLS) (to M.J.F.; Project-ID DJCLS 01ZI/2022). This work has been supported by grant support from the International Myeloma Society (to P.N. and M.-S.R.) and a Pfizer translational grant (to N.J.B.). This work has been supported by the Terry Fox Research Institute (M4 Study Project 10017712 to N.J.B.). We thank the Dietmar Hopp Stiftung GmbH (1DH118373, University Hospital Heidelberg und 1DH1911364, German Cancer Research Center) for providing funding for this study. This work has also been supported by the German Cancer Aid (to M.P.; Project-ID 70113515). M.J.F. is a member of the MD/PhD program at Heidelberg University. M.J.F. is a fellow of the German Research Foundation (DFG). N.K. received fellowships by the German Academic Scholarship Foundation and the Research Training Group (RTG) 2099 funded by the DFG (Project-ID 259332240). J.M. received a fellowship by the German Cancer Aid (Project-ID 70114336). M.K. received fellowships by Helmholtz International Graduate School for Cancer Research and the Landesgraduiertenförderung (LGF). R.S. was funded by the Else Kroner-Fresenius Foundation.

AUTHOR CONTRIBUTIONS

M.J.F. conceptualized the study, designed and performed experiments, analyzed and interpreted data, and wrote the paper. P.N. performed experiments, interpreted data, and wrote the paper. N.K. and J.M. analyzed scRNA-seq data and performed experiments. N.L., R.M., and S.A. performed single-cell experiments. H.L. and E.B analyzed the data. S.S. and K.R. performed TCR clone tracing and RNA velocity analyses. R.S. performed cell-cell interaction analyses. L.B., M.P., C.M.-T., and H.G. were involved in study design and data interpretation. M.-S.R. and N.J.B. supervised the study and interpreted data.

DECLARATION OF INTERESTS

The authors declare that the research was conducted in the absence of any commercial or financial relationships that could be construed as a potential conflict of interest. P.N. reports receiving speaker's bureau honoraria from BMS, Janssen, and Sanofi, and is a consultant/advisory board member for BMS and Janssen. C.M.-T. received research funding from Pfizer and BiolineRX. M.-S.R. reports receiving speaker's bureau honoraria from Amgen, BMS, Sanofi, and Janssen, and is a consultant/advisory board member for BMS, GSK, Amgen, Janssen, and Pfizer. He received research funding from Amgen, Sanofi, and Janssen. N.J.B. reports receiving speaker's bureau honoraria from Amgen, BMS, Sanofi, Pfizer, and Janssen, and is a consultant/advisory board member for BMS, Janssen, and Pfizer. All other authors declare no competing interests.

INCLUSION AND DIVERSITY

One or more of the authors of this paper self-identifies as an underrepresented ethnic minority in their field of research or within their geographical location. One or more of the authors of this paper self-identifies as a member of the LGBTQIA+ community. One or more of the authors of this paper received support from a program designed to increase minority representation in their field of research.

Received: May 20, 2022
Revised: November 2, 2022
Accepted: February 8, 2023
Published: March 9, 2023

REFERENCES

1. Waldman, A.D., Fritz, J.M., and Lenardo, M.J. (2020). A guide to cancer immunotherapy: from T cell basic science to clinical practice. Nat. Rev. Immunol. *20*, 651–668. https://doi.org/10.1038/s41577-020-0306-5.

2. June, C.H., O'Connor, R.S., Kawalekar, O.U., Ghassemi, S., and Milone, M.C. (2018). CAR T cell immunotherapy for human cancer. Science *359*, 1361–1365. https://doi.org/10.1126/science.aar6711.

3. Carpen, L., Falvo, P., Orecchioni, S., Mitola, G., Hillje, R., Mazzara, S., Mancuso, P., Pileri, S., Raveane, A., and Bertolini, F. (2022). A single-cell transcriptomic landscape of innate and adaptive intratumoral immunity in triple negative breast cancer during chemo- and immunotherapies. Cell Death Dis. *8*, 106. https://doi.org/10.1038/S41420-022-00893-X.

4. Bassez, A., Vos, H., van Dyck, L., Floris, G., Arijs, I., Desmedt, C., Boeckx, B., vanden Bempt, M., Nevelsteen, I., Lambein, K., et al. (2021). A single-cell map of intratumoral changes during anti-PD1 treatment of patients with breast cancer. Nat. Med. *27*, 820–832. https://doi.org/10.1038/s41591-021-01323-8.

5. Liu, B., Hu, X., Feng, K., Gao, R., Xue, Z., Zhang, S., Zhang, Y., Corse, E., Hu, Y., Han, W., and Zhang, Z. (2021). Temporal single-cell tracing reveals clonal revival and expansion of precursor exhausted T cells during anti-PD-1 therapy in lung cancer. Nat. Can. (Que.) *3*, 108–121. https://doi.org/10.1038/s43018-021-00292-8.

6. Oliveira, G., Stromhaug, K., Klaeger, S., Kula, T., Frederick, D.T., Le, P.M., Forman, J., Huang, T., Li, S., Zhang, W., et al. (2021). Phenotype, specificity and avidity of antitumour CD8+ T cells in melanoma. Nature *596*, 7870. https://doi.org/10.1038/s41586-021-03704-y.

7. Scheper, W., Kelderman, S., Fanchi, L.F., Linnemann, C., Bendle, G., de Rooij, M.A.J., Hirt, C., Mezzadra, R., Slagter, M., Dijkstra, K., et al. (2019). Low and variable tumor reactivity of the intratumoral TCR repertoire in human cancers. Nat. Med. *25*, 89–94. https://doi.org/10.1038/s41591-018-0266-5.

8. Zavidij, O., Haradhvala, N.J., Mouhieddine, T.H., Sklavenitis-Pistofidis, R., Cai, S., Reidy, M., Rahmat, M., Flaifel, A., Ferland, B., Su, N.K., et al. (2020). Single-cell RNA sequencing reveals compromised immune microenvironment in precursor stages of multiple myeloma. Nat. Can. (Que.) *1*, 493–506. https://doi.org/10.1038/s43018-020-0053-3.

9. Liu, R., Gao, Q., Foltz, S.M., Fowles, J.S., Yao, L., Wang, J.T., Cao, S., Sun, H., Wendl, M.C., Sethuraman, S., et al. (2021). Co-evolution of tumor and immune cells during progression of multiple myeloma. Nat. Commun. *12*, 2559. https://doi.org/10.1038/s41467-021-22804-x.

10. Ledergor, G., Weiner, A., Zada, M., Wang, S.Y., Cohen, Y.C., Gatt, M.E., Snir, N., Magen, H., Koren-Michowitz, M., Herzog-Tzarfati, K., et al. (2018). Single cell dissection of plasma cell heterogeneity in symptomatic and asymptomatic myeloma. Nat. Med. *24*, 1867–1876.

11. Tirier, S.M., Mallm, J.P., Steiger, S., Poos, A.M., Awwad, M.H.S., Giesen, N., Casiraghi, N., Susak, H., Bauer, K., Baumann, A., et al. (2021). Subclone-specific microenvironmental impact and drug response in refractory multiple myeloma revealed by single-cell transcriptomics. Nat. Commun. *12*, 6960. https://doi.org/10.1038/s41467-021-26951-z.

12. de Jong, M.M.E., Kellermayer, Z., Papazian, N., Tahri, S., Hofste op Bruinink, D., Hoogenboezem, R., Sanders, M.A., van de Woestijne, P.C., Bos, P.K., Khandanpour, C., et al. (2021). The multiple myeloma microenvironment is defined by an inflammatory stromal cell landscape. Nat. Immunol. *22*, 769–780. https://doi.org/10.1038/s41590-021-00931-3.

13. Bailur, J.K., McCachren, S.S., Doxie, D.B., Shrestha, M., Pendleton, K., Nooka, A.K., Neparidze, N., Parker, T.L., Bar, N., Kaufman, J.L., et al. (2019). Early alterations in stem-like/marrow-resident T cells and innate and myeloid cells in preneoplastic gammopathy. JCI Insight *5*, e127807. https://doi.org/10.1172/JCI.INSIGHT.127807.

14. Baccin, C., Al-Sabah, J., Velten, L., Helbling, P.M., Grünschläger, F., Hernández-Malmierca, P., Nombela-Arrieta, C., Steinmetz, L.M., Trumpp, A., and Haas, S. (2020). Combined single-cell and spatial transcriptomics reveal the molecular, cellular and spatial bone marrow niche organization. Nat. Cell Biol. *22*, 38–48. https://doi.org/10.1038/S41556-019-0439-6.

15. Dolgalev, I., and Tikhonova, A.N. (2021). Connecting the dots: resolving the bone marrow niche heterogeneity. Front. Cell Dev. Biol. *9*, 478. https://doi.org/10.3389/FCELL.2021.622519/BIBTEX.

16. Baryawno, N., Przybylski, D., Kowalczyk, M.S., Kfoury, Y., Severe, N., Gustafsson, K., Kokkaliaris, K.D., Mercier, F., Tabaka, M., Hofree, M., et al. (2019). A cellular taxonomy of the bone marrow stroma in homeostasis and leukemia. Cell *177*, 1915–1932.e16. https://doi.org/10.1016/J.CELL.2019.04.040.

17. Yost, K.E., Satpathy, A.T., Wells, D.K., Qi, Y., Wang, C., Kageyama, R., McNamara, K.L., Granja, J.M., Sarin, K.Y., Brown, R.A., et al. (2019). Clonal replacement of tumor-specific T cells following PD-1 blockade. Nat. Med. *25*, 1251–1259. https://doi.org/10.1038/s41591-019-0522-3.

18. Sade-Feldman, M., Yizhak, K., Bjorgaard, S.L., Ray, J.P., de Boer, C.G., Jenkins, R.W., Lieb, D.J., Chen, J.H., Frederick, D.T., Barzily-Rokni, M., et al. (2018). Defining T cell states associated with response to checkpoint immunotherapy in melanoma. Cell *175*, 998–1013.e20. https://doi.org/10.1016/j.cell.2018.10.038.

19. Li, H., van der Leun, A.M., Yofe, I., Lubling, Y., Gelbard-Solodkin, D., van Akkooi, A.C.J., van den Braber, M., Rozeman, E.A., Haanen, J., Blank, C.U., et al. (2019). Dysfunctional CD8 T cells form a proliferative, dynamically regulated compartment within human melanoma. Cell *176*, 775–789.e18. https://doi.org/10.1016/j.cell.2018.11.043.

20. Mcgranahan, N., Furness, A.J.S., Rosenthal, R., Ramskov, S., Lyngaa, R., Saini, S.K., Jamal-hanjani, M., Wilson, G.A., Birkbak, N.J., Hiley, C.T., et al. (2016). Clonal neoantigens elicit T cell immunoreactivity and sensitivity to immune checkpoint blockade. Science *351*, 1463–1469. https://doi.org/10.1126/science.aaf1490.

21. Horton, B.L., Morgan, D.M., Momin, N., Zagorulya, M., Torres-Meji, E., Bhandarkar, V., Wittrup, K.D., Love, J.C., and Spranger, S. (2021). Lack of CD8+T cell effector differentiation during priming mediates checkpoint blockade resistance in non-small cell lung cancer. Sci Immunol *6*. https://doi.org/10.1126/SCIIMMUNOL.ABI8800/SUPPL_FILE/SCIIMMUNOL.ABI8800_MOVIES_S1_TO_S4.ZIP.

22. Pittet, M.J., Michielin, O., and Migliorini, D. (2022). Clinical relevance of tumour-associated macrophages. Nat. Rev. Clin. Oncol. *19*, 402–421. https://doi.org/10.1038/S41571-022-00620-6.

23. Beatty, G.L., and Gladney, W.L. (2015). Immune escape mechanisms as a guide for cancer immunotherapy. Clin. Cancer Res. *21*, 687–692. https://doi.org/10.1158/1078-0432.CCR-14-1860.

24. Verkleij, C.P.M., Broekmans, M.E.C., van Duin, M., Frerichs, K.A., Kuiper, R., de Jonge, A.V., Kaiser, M., Morgan, G., Axel, A., Boominathan, R., et al. (2021). Preclinical activity and determinants of response of the GPRC5DxCD3 bispecific antibody talquetamab in multiple myeloma. Blood Adv. *5*, 2196–2215. https://doi.org/10.1182/bloodadvances.2020003805.

25. Pillarisetti, K., Powers, G., Luistro, L., Babich, A., Baldwin, E., Li, Y., Zhang, X., Mendonça, M., Majewski, N., Nanjunda, R., et al. (2020). Teclistamab is an active T cell-redirecting bispecific antibody against B-cell maturation antigen for multiple myeloma. Blood Adv. *4*, 4538–4549. https://doi.org/10.1182/BLOODADVANCES.2020002393.

26. Garfall, A.L., Usmani, S.Z., Mateos, M.-V., Nahi, H., van de Donk, N.W., San-Miguel, J.F., Oriol Rocafiguera, A., Rosinol, L., Chari, A., Bhutani, M., et al. (2020). Updated phase 1 results of teclistamab, a B-cell maturation antigen (BCMA) x CD3 bispecific antibody, in relapsed and/or refractory multiple myeloma (RRMM). Blood *136*, 27. https://doi.org/10.1182/blood-2020-138831.

27. Harrison, S.J., Minnema, M.C., Lee, H.C., Spencer, A., Kapoor, P., Madduri, D., Larsen, J., Ailawadhi, S., Kaufman, J.L., Raab, M.S., et al. (2020). A phase 1 first in human (FIH) study of AMG 701, an anti-B-cell maturation antigen (BCMA) half-life extended (HLE) BiTE® (bispecific

T-cell engager) molecule, in relapsed/refractory (RR) multiple myeloma (MM). Blood *136*. https://doi.org/10.1182/blood-2020-134063.

28. Bahlis, N.J., Raje, N.S., Costello, C., Dholaria, B.R., Solh, M.M., Levy, M.Y., Tomasson, M.H., Dube, H., Liu, F., Liao, K.H., et al. (2021). Efficacy and Safety of Elranatamab (PF-06863135), a B-Cell Maturation Antigen (BCMA)-CD3 Bispecific Antibody, in Patients with Relapsed or Refractory Multiple Myeloma (MM). J. Clin. Oncol. *39*. 8006–8006. https://doi.org/10.1200/JCO.2021.39.15_suppl.8006.

29. Verkleij, C.P.M., Frerichs, K.A., Broekmans, M., Absalah, S., Maas-Bosman, P.W.C., Kruyswijk, S., Nijhof, I.S., Mutis, T., Zweegman, S., and van de Donk, N. (2020). T-cell redirecting bispecific antibodies targeting BCMA for the treatment of multiple myeloma. Oncotarget *11*, 4076–4081. https://doi.org/10.18632/oncotarget.27792.

30. Truger, M.S., Duell, J., Zhou, X., Heimeshoff, L., Ruckdeschel, A., John, M., Riedel, A., Hüper, S., Peter, J., Walter, W., et al. (2021). Single- and double-hit events in genes encoding immune targets before and after T cell-engaging antibody therapy in MM. Blood Adv. *5*, 3794–3798. https://doi.org/10.1182/BLOODADVANCES.2021004418.

31. Alrasheed, N., Lee, L., Ghorani, E., Henry, J.Y., Conde, L., Chin, M., Galas-Filipowicz, D., Furness, A.J.S., Chavda, S.J., Richards, H., et al. (2020). Marrow-infiltrating regulatory T cells correlate with the presence of dysfunctional CD4þPD-1þ cells and inferior survival in patients with newly diagnosed multiple myeloma. Clin. Cancer Res. *26*, 3443–3454. https://doi.org/10.1158/1078-0432.CCR-19-1714.

32. Prabhala, R.H., Neri, P., Bae, J.E., Tassone, P., Shammas, M.A., Allam, C.K., Daley, J.F., Chauhan, D., Blanchard, E., Thatte, H.S., et al. (2006). Dysfunctional T regulatory cells in multiple myeloma. Blood *107*, 301–304. https://doi.org/10.1182/blood-2005-08-3101.

33. Koike, M., Sekigawa, I., Okada, M., Matsumoto, M., Iida, N., Hashimoto, H., and Oshimi, K. (2002). Relationship between CD4+/CD8+ T cell ratio and T cell activation in multiple myeloma: reference to IL-16. Leuk. Res. *26*, 705–711. https://doi.org/10.1016/S0145-2126(01)00192-8.

34. Redoglia, V., Boccadoro, M., Battaglio, S., Dianzani, U., Massaia, M., and Pileri, A. (1990). Multiple myeloma: altered CD4/CD8 ratio in bone marrow. Haematologica *75*, 129–131.

35. Galletti, G., de Simone, G., Mazza, E.M.C., Puccio, S., Mezzanotte, C., Bi, T.M., Davydov, A.N., Metsger, M., Scamardella, E., Alvisi, G., et al. (2020). Two subsets of stem-like CD8+ memory T cell progenitors with distinct fate commitments in humans. Nat. Immunol. *21*, 1552–1562. https://doi.org/10.1038/s41590-020-0791-5.

36. Seckinger, A., Delgado, J.A., Moser, S., Moreno, L., Neuber, B., Grab, A., Lipp, S., Merino, J., Prosper, F., Emde, M., et al. (2017). Target expression, generation, preclinical activity, and pharmacokinetics of the BCMA-T cell bispecific antibody EM801 for multiple myeloma treatment. Cancer Cell *31*, 396–410. https://doi.org/10.1016/J.CCELL.2017.02.002.

37. Ross, T., Reusch, U., Wingert, S., Haneke, T., Klausz, K., Otte, A.-K., Schub, N., Knackmuss, S., Müller, T., Ellwanger, K., et al. (2018). Preclinical characterization of AFM26, a novel B cell maturation antigen (BCMA)-Directed tetravalent bispecific antibody for high affinity retargeting of NK cells against myeloma. Blood *132*, 1927. https://doi.org/10.1182/BLOOD-2018-99-118970.

38. Watkins-Yoon, J., Guzman, W., Oliphant, A., Haserlat, S., Leung, A., Chottin, C., Ophir, M., Vekeria, J., Nelson, A.P., Frye, Z., et al. (2019). CTX-8573, an innate-cell engager targeting BCMA, is a highly potent multispecific antibody for the treatment of multiple myeloma. Blood *134*, 3182. https://doi.org/10.1182/BLOOD-2019-128749.

39. Kodama, T., Kochi, Y., Nakai, W., Mizuno, H., Baba, T., Habu, K., Sawada, N., Tsunoda, H., Shima, T., Miyawaki, K., et al. (2019). Anti-GPRC5D/CD3 bispecific T-cell-redirecting antibody for the treatment of multiple myeloma. Mol. Cancer Therapeut. *18*, 1555–1564. https://doi.org/10.1158/1535-7163.MCT-18-1216.

40. Pillarisetti, K., Edavettal, S., Mendonça, M., Li, Y., Tornetta, M., Babich, A., Majewski, N., Husovsky, M., Reeves, D., Walsh, E., et al. (2020). A T-cell–redirecting bispecific G-protein–coupled receptor class 5 member D x CD3 antibody to treat multiple myeloma. Blood *135*, 1232–1243. https://doi.org/10.1182/BLOOD.2019003342.

41. Frerichs, K.A., Broekmans, M.E.C., Marin Soto, J.A., van Kessel, B., Heymans, M.W., Holthof, L.C., Verkleij, C.P.M., Boominathan, R., Vaidya, B., Sendecki, J., et al. (2020). Preclinical activity of JNJ-7957, a novel BCMA ×CD3 bispecific antibody for the treatment of multiple myeloma, is potentiated by daratumumab. Clin. Cancer Res. *26*, 2203–2215. https://doi.org/10.1158/1078-0432.CCR-19-2299.

42. Li, Z., Li, Q., Zhang, G., Ma, X., Li, Z., Hu, X., Ouyang, K., Li, B., and Liu, Z. (2019). A Novel bispecific BCMAxCD3 T cell-engaging antibody that treat multiple myeloma (MM) with minimal cytokine secretion. Ann. Oncol. *30*, v808. https://doi.org/10.1093/ANNONC/MDZ269.038.

43. Fayon, M., Martinez-Cingolani, C., Abecassis, A., Roders, N., Nelson, E., Choisy, C., Talbot, A., Bensussan, A., Fermand, J.P., Arnulf, B., and Bories, J.C. (2021). Bi38-3 is a novel CD38/CD3 bispecific T-cell engager with low toxicity for the treatment of multiple myeloma. Haematologica *106*, 1193–1197. https://doi.org/10.3324/HAEMATOL.2019.242453.

44. Gantke, T., Reusch, U., Kellner, C., Ellwanger, K., Fucek, I., Weichel, M., Kerber, A., Peipp, M., and Treder, M. (2017). AFM26 is a novel, highly potent BCMA/CD16A-directed bispecific antibody for high affinity NK-cell engagement in multiple myeloma. J. Clin. Oncol. *35*, 8045. https://doi.org/10.1200/JCO.2017.35.15_SUPPL.8045.

45. Carpenter, R.O., Evbuomwan, M.O., Pittaluga, S., Rose, J.J., Raffeld, M., Yang, S., Gress, R.E., Hakim, F.T., and Kochenderfer, J.N. (2013). B-cell maturation antigen is a promising target for adoptive T-cell therapy of multiple myeloma. Clin. Cancer Res. *19*, 2048–2060. https://doi.org/10.1158/1078-0432.CCR-12-2422.

46. Lancman, G., Sastow, D.L., Cho, H.J., Jagannath, S., Madduri, D., Parekh, S.S., Richard, S., Richter, J., Sanchez, L., Chari, A., et al. (2021). Bispecific antibodies in multiple myeloma: present and future. Blood Cancer Discov. *2*, 423–433. https://doi.org/10.1158/2643-3230.BCD-21-0028.

47. Mogilenko, D.A., Shpynov, O., Andhey, P.S., Arthur, L., Swain, A., Esaulova, E., Brioschi, S., Shchukina, I., Kerndl, M., Bambouskova, M., et al. (2021). Comprehensive profiling of an aging immune system reveals clonal GZMK+ CD8+ T cells as conserved hallmark of inflammaging. Immunity *54*, 99–115.e12. https://doi.org/10.1016/j.immuni.2020.11.005.

48. Pilcher, W., Thomas, B.E., Bhasin, S.S., Jayasinghe, R.G., Rahman, A.H., Kim-Schulze, S., Gonzalez-Kozlova, E., Kourelis, T., Dhodapkar, M.V., Vij, R., et al. (2021). Characterization of T-cell exhaustion in rapid progressing multiple myeloma using cross center Scrna-seq study. Blood *138*, 401. https://doi.org/10.1182/blood-2021-153863.

49. Lange, M., Bergen, V., Klein, M., Setty, M., Reuter, B., Bakhti, M., Lickert, H., Ansari, M., Schniering, J., Schiller, H.B., et al. (2022). CellRank for directed single-cell fate mapping. Nat. Methods *19*, 159–170. https://doi.org/10.1038/s41592-021-01346-6.

50. Velten, L., Haas, S.F., Raffel, S., Blaszkiewicz, S., Islam, S., Hennig, B.P., Hirche, C., Lutz, C., Buss, E.C., Nowak, D., et al. (2017). Human haematopoietic stem cell lineage commitment is a continuous process. Nat. Cell Biol. *19*, 271–281. https://doi.org/10.1038/NCB3493.

51. Wrapp, D., Wang, N., Corbett, K.S., Goldsmith, J.A., Hsieh, C.L., Abiona, O., Graham, B.S., McLellan, J.S., Lee, G.R., Li, H.B., et al. (2020). MRNA destabilization by BTG1 and BTG2 maintains T cell quiescence. Science *367*, 1260–1263. https://doi.org/10.1126/SCIENCE.ABB2507.

52. Fernández de Larrea, C., Staehr, M., Lopez, A.V., Ng, K.Y., Chen, Y., Godfrey, W.D., Purdon, T.J., Ponomarev, V., Wendel, H.-G., Brentjens, R.J., and Smith, E.L. (2020). Defining an optimal dual-targeted CAR T-cell therapy approach simultaneously targeting BCMA and GPRC5D to prevent BCMA escape–driven relapse in multiple myeloma. Blood Cancer Discov. *1*, 146–154. https://doi.org/10.1158/2643-3230.BCD-20-0020.

53. Church, S.E., Jensen, S.M., Antony, P.A., Restifo, N.P., and Fox, B.A. (2014). Tumor-specific CD4+ T cells maintain effector and memory

tumor-specific CD8+ T cells. Eur. J. Immunol. *44*, 69–79. https://doi.org/10.1002/eji.201343718.

54. Borst, J., Ahrends, T., Bąbała, N., Melief, C.J.M., and Kastenmüller, W. (2018). CD4+ T cell help in cancer immunology and immunotherapy. Nat. Rev. Immunol. *18*, 635–647. https://doi.org/10.1038/s41577-018-0044-0.

55. Meermeier, E.W., Welsh, S.J., Sharik, M.E., Du, M.T., Garbitt, V.M., Riggs, D.L., Shi, C.X., Stein, C.K., Bergsagel, M., Chau, B., et al. (2021). Tumor burden limits bispecific antibody efficacy through T-cell exhaustion averted by concurrent cytotoxic therapy. Blood Cancer Discov. *2*, 354–369. https://doi.org/10.1158/2643-3230.BCD-21-0038.

56. Zitvogel, L., and Kroemer, G. (2021). Bortezomib induces immunogenic cell death in multiple myeloma. Blood Cancer Discov. *2*, 405–407. https://doi.org/10.1158/2643-3230.BCD-21-0059.

57. Gulla, A., Morelli, E., Samur, M.K., Botta, C., Hideshima, T., Bianchi, G., Fulciniti, M., Malvestiti, S., Prabhala, R.H., Talluri, S., et al. (2021). Bortezomib induces anti-multiple myeloma immune response mediated by cGAS/STING pathway activation. Blood Cancer Discov. *2*, 468–483. https://doi.org/10.1158/2643-3230.BCD-21-0047.

58. Chiriva-Internati, M., Grizzi, F., Pinkston, J., Morrow, K.J., D'Cunha, N., Frezza, E.E., Muzzio, P.C., Kast, W.M., and Cobos, E. (2006). Gamma-radiation upregulates MHC class I/II and ICAM-I molecules in multiple myeloma cell lines and primary tumors. In Vitro Cell. Dev. Biol. Anim. *42*, 89–95. https://doi.org/10.1290/0508054.1.

59. Laydon, D.J., Bangham, C.R., and Asquith, B. (2015). Estimating T-cell repertoire diversity: limitations of classical estimators and a new approach. Philos Trans R Soc Lond B Biol Sci. *370*, 20140291. https://doi.org/10.1098/rstb.2014.0291.

60. Datlinger, P., Rendeiro, A.F., Boenke, T., Senekowitsch, M., Krausgruber, T., Barreca, D., and Bock, C. (2021). Ultra-high-throughput single-cell RNA sequencing and perturbation screening with combinatorial fluidic indexing. Nat. Methods *18*, 635–642. https://doi.org/10.1038/s41592-021-01153-z.

STAR★METHODS

KEY RESOURCES TABLE

REAGENT or RESOURCE	SOURCE	IDENTIFIER
Antibodies		
CD45 PerCP-Cy5.5	BD	564106
CD3 FITC	BD	555916
CD4 PE	ThermoFisher	12-0048-42
CD8 APC	BD	340584
CD138 APC-R700	BD	566050
CD269 (BCMA) PE	BioLegend	357504
CD38 FITC	BD	340909
CD138 V500-C	BD	650659
HLA A,B,C APC	BioLegend	311410
MHC-II BUV615	ThermoFisher	366-9956-42
Human TruStain FcX™ (Fc Receptor Blocking Solution)	BioLegend	422302
TotalSeq™-C0251 anti-human Hashtag 1 Antibody	BioLegend	394661
TotalSeq™-C0252 anti-human Hashtag 2 Antibody	BioLegend	394663
TotalSeq™-C0253 anti-human Hashtag 3 Antibody	BioLegend	394665
TotalSeq™-C0254 anti-human Hashtag 4 Antibody	BioLegend	394667
TotalSeq™-C0256 anti-human Hashtag 6 Antibody	BioLegend	394671
TotalSeq™-C0257 anti-human Hashtag 7 Antibody	BioLegend	394673
TotalSeq™-C0258 anti-human Hashtag 8 Antibody	BioLegend	394675
TotalSeq™-C0259 anti-human Hashtag 9 Antibody	BioLegend	394677
HLA-ABC Monoclonal Antibody (W6/32)	Life Science Technologies	MA1-19027
Recombinant Anti-BCMA x Anti-CD3 CrossMab Bispecific Antibody	CreativeBiolabs	CROSSAB-H198
Biological samples		
Human bone marrow cells	Primary samples	N/A
Human peripheral blood cells	Primary samples	N/A
Chemicals, peptides, and recombinant proteins		
DPBS	Gibco	14190-094
BSA	SIGMA	A9647-100G
DMSO	ThermoFisher Scientific	13494279
RPMI-1640 Medium	Gibco	61870-010
ImmunoCult-XF T Cell Expansion Medium	STEMCELL technologies	10981
human IL-2	PeproTech	200-02
human IL-7	Miltenyi Biotec	130-095-362
human IL-15	Miltenyi Biotec	130-095-764
CEFT Pool ,120nmol >70%	JPT Peptide Technologies	PM-CEFT-2
Critical commercial assays		
CD138 MicroBeads, human	Miltenyi Biotec	130-051-301
Pan T cell isolation kit, human	Miltenyi Biotec	130-096-535
Chromium Next GEM Single Cell 5′ v2 Dual Indexing assay	10x Genomics	PN-1000263 PN-1000254 PN-1000286 PN-1000215

(*Continued on next page*)

Continued

REAGENT or RESOURCE	SOURCE	IDENTIFIER
Deposited data		
Raw single-cell sequencing dataset	This paper	Gene Expression Omnibus (GEO): GSE217245
Processed single-cell sequencing dataset	This paper	Gene Expression Omnibus (GEO): GSE216571
Healthy bone marrow donor single-cell sequencing dataset	Zavidij et al.,[8] Nat Cancer 2020 May; 1(5):493–506. PMID: 33409501	Gene Expression Omnibus (GEO): GSE124310
Deep VDJ-seq dataset	Adaptive Biotechnologies immuneACCESS® database	https://doi.org/10.21417/MJF2022CC
Software and algorithms		
R v4.1.0	The R Foundation	N/A
GraphPad Prism v9.0	GraphPad Software Inc.	N/A
FACSDiva v6.1	BD Biosciences	N/A
Seurat_4.0.3		https://github.com/satijalab/seurat
harmony_0.1.0	https://doi.org/10.1016/j.cell.2021.04.048	https://github.com/immunogenomics/harmony
symphony_0.1.0	https://doi.org/10.1038/s41592-019-0619-0	https://github.com/immunogenomics/symphony
scRepertoire_1.3.1	https://doi.org/10.1101/2020.11.18.389189	https://github.com/ncborcherding/scRepertoire
ggplot2_3.3.5	http://bioconductor.org/packages/release/bioc/html/scRepertoire.html	https://github.com/tidyverse/ggplot2
dplyr_1.0.7		https://github.com/tidyverse/dplyr
CellRank_1.5.1	https://doi.org/10.1038/s41592-021-01346-6	https://cellrank.readthedocs.io/en/stable/
CellPhoneDB_2.1.7	https://doi.org/10.1038/s41596-020-0292-x	https://github.com/Teichlab/cellphonedb
velocyto.py_0.17	https://doi.org/10.1038/s41586-018-0414-6	http://velocyto.org/velocyto.py/
scanpy_1.8.2	https://doi.org/10.1186/s13059-017-1382-0	https://scanpy.readthedocs.io/
scVelo_0.2.4	https://doi.org/10.1038/s41587-020-0591-3	https://scvelo.readthedocs.io/
DescTools_0.99.44		https://github.com/AndriSignorell/DescTools/
tidymodels_1.0.0		https://tidymodels.org
rsample_1.1.0		https://CRAN.R-project.org/package=rsample

RESOURCE AVAILABILITY

Lead contact

Further information and requests for resources should be directed to and will be fulfilled by Mirco Friedrich (mfriedri@broadinstitute.org).

Materials availability

This study did not generate new unique reagents

Data and code availability

- Raw single-cell sequencing data used in this study are publicly available at Gene Expression Omnibus (GEO) under accession number GSE217245.
- Processed single-cell sequencing data used in this study are publicly available at Gene Expression Omnibus (GEO) under accession number GSE216571.
- Single-cell sequencing data from HBM and NDMM patients that were reanalyzed within this study are publicly available at Gene Expression Omnibus (GEO) under accession number GSE124310.
- Deep VDJ-seq data have been deposited in the Adaptive Biotechnologies immuneACCESS® database (https://doi.org/10.21417/MJF2022CC).
- Any additional information required to reanalyze the data reported in this paper is available from the lead contact upon request.

EXPERIMENTAL MODEL AND SUBJECT DETAILS

Human patients

This study was approved by the University of Calgary Institutional review board and all patients provided written informed consent for tumor sequencing and review of patient medical records for detailed demographic, pathologic, and treatment information (Ethics ID: HREBA.CC-21-0248). Characteristics of each subject included are available in Table S1. Written informed consent was obtained by all patients and donors prior to this study conformed to the principles set out in the WMA Declaration of Helsinki and in the Department of Health and Human Services Belmont Report. The patient specimens collected within this study were collected from an ongoing prospective clinical trial (NCT03269136), however the correlative studies performed here are from a parallel independently approved research project by the sponsor (Pfizer grant 68247815 to N. Bahlis). The data therefore do not represent a planned interim analysis. Ethical approval for the isolation and functional testing of bone marrow aspirates, and peripheral blood for *in vitro* experiments was obtained from the Heidelberg Medical Faculty Ethics Committee (Reference number S-096/2017).

METHOD DETAILS

Processing of human bone marrow samples

Bone marrow aspirates were 1:1 diluted in preparation buffer (PBS with 0.1% BSA and 2 mM EDTA), and mononuclear cell separation was performed by density centrifugation (Bicoll separating solution, Biochrom) with diluted bone marrow cells (centrifugation 20 min, 1300g). Cells were carefully aspirated and washed with preparation buffer (centrifugation 5 min at 470g). Red blood cells were lysed using RCL buffer (155 mM NH4Cl, 10 mM KHCO3, 0.1 mM EDTA) for 10 min at room temperature and bone marrow cells were washed (centrifugation 5 min, 470g) and resuspended in preparation buffer. Malignant plasma cells were freshly isolated using CD138 MicroBeads, human (Miltenyi Biotec) according to the manufacturer's instructions and frozen in 90% FCS (Sigma-Aldrich) supplemented with 10% DMSO and stored in liquid nitrogen until further use. Non-plasma bone marrow mononuclear cells were frozen after cell counting at 1×10^7 cells per aliquot in 90% FCS (Sigma-Aldrich) supplemented with 10% DMSO and stored in liquid nitrogen until further use.

Processing of human peripheral blood samples

Peripheral blood samples were 1:1 diluted in preparation buffer (PBS with 0.1% BSA and 2 mM EDTA), and mononuclear cell separation was performed by density centrifugation (Bicoll separating solution, Biochrom) with diluted peripheral blood cells (centrifugation 20 min, 1300g). Cells were carefully aspirated and washed with preparation buffer (centrifugation 5 min at 470g). Red blood cells were lysed using RCL buffer (155 mM NH4Cl, 10 mM KHCO3, 0.1 mM EDTA) for 1 min at room temperature and cells were washed (centrifugation 5 min, 470g) and resuspended in preparation buffer. After cell counting, 1×10^7 cells were frozen per aliquot in 90% FCS (Sigma-Aldrich) supplemented with10 % DMSO and stored in liquid nitrogen until further use.

Single-cell RNA sequencing and data preprocessing

Our protocol used viably frozen cells that were thawed at 37°C, resuspended in ice-cold PBS and washed twice with cells being collected by centrifugation at 500g for 4 min. The freezing step had little effect on data quality, major cell-type composition and transcriptome as evaluated by us previously (Tirier et al. 2021). Thawed cells were counted, split in 8 aliquots per patient sample and separately stained with TotalSeq™ hashtag antibodies (BioLegend) and fluorescently labeled antibodies before pooling for flow cytometry. Viable, $CD45^+$ or $CD45^+$ $CD3^+$ cells were isolated by fluorescence-activated cell sorting (Figure S1A) Single-cell capture, reverse transcription, and library preparation were carried out on the Chromium platform (10x Genomics) with the Single Cell 5' reagent v2 kit (10x Genomics) according to the manufacturer's protocol using 40,000 cells as input per channel. Each pool of cells was tested for library quality and library concentration was assessed. Each of the final libraries were paired-end sequenced (26 and 92 bp) on one Illumina NovaSeq 6000 S2 lane. Raw sequencing data were processed and aligned to the human genome (GRCh38) using the CellRanger pipeline (10x Genomics, version 6.0).

Single-cell transcriptomic analyses

Quality control and normalization

Control datasets for heathy bone marrow and newly diagnosed myeloma were accessed under the GEO accession series GSE124310 and processed alongside the newly generated datasets.

Single-cell RNA data were processed using the CellRanger pipeline (version 6.0) to the GRChg38 reference genome with all default settings. All cells which had unique feature counts over 2,500 (RunB & Control) / 4000 (RunA) or less than 200 (RunB & Control) / 500 (RunA) as well as >10% mitochondrial counts were excluded from the analysis. In addition, genes detected in fewer than three cells were excluded from downstream analysis. Samples were split in 8 aliquots and separately stained with single TotalSeq™ hashtag antibodies (BioLegend) as well as fluorescently labeled antibodies before pooling for flow cytometry. These fractions were demultiplexed and cells were classified as Hashtag+ singlets, doublets or unassigned cells using the HTODemux command with default settings (Stoeckius et al., Genome Biology 2018; https://genomebiology.biomedcentral.com/articles/10.1186/s13059-018-1603-1. Cells without an assigned hashtag (unassigned cells) or doublets were removed. Subsequently, only cells classified as singlets (67.8%) were used for further analyses. We provided the corresponding heatmap and quantification under Figure S1B. Gene

expression was normalized using Seurat's LogNormalization() and highly variable genes were identified by using the FindVariableFeatures(). VDJ data was added using the combineExpression() function from scRepertoire V.1.3.1. by using the amino acid sequence (CTaa) for clonotype calling. Downstream analyses of TCE patients was performed on all cells with detected TCR alpha- and beta-chains (248,478 T cells; 63,374 TCR clonotypes).

Analysis of bone marrow immune cells for cell cell interaction analyses

After preprocessing and QC, all patient datasets were mapped onto the CITE-seq reference of human bone marrow mononuclear cells (BMNC) using the MapQuery function in Seurat. We used the CITE-seq dataset from (Stuart*, Butler* et al, Cell 2019), which consists of 30,672 scRNA-seq profiles measured alongside a panel of 25 antibodies from bone marrow. The performed reference mapping using default parameters by finding anchors between each of our datasets with the query dataset via FindTransferAnchors() according to the published vignette (https://satijalab.org/seurat/articles/multimodal_reference_mapping.html). T cells were identified based on CITE-seq reference mapping.

Integration of TCE patient datasets and timepoints

T cells from $CD3^+$ sorted samples subsetted based on the CITE-seq reference above were analyzed and integrated by using the Harmony V0.1.0 package according to the published vignette. Normalization was done by LogNormalize() and FindVariableFeatures generating 2500 Variable features. Subsequently batch effect-associated features as well as immune-receptor variable genes (JUN|FOS|RP|ZFP36|EGR|HSP|MALAT1|XIST|MT-|HIST|TRAV|TRAD|TRAJ|TRBV|TRBD|TRBJ|TRGV|TRGD|TRGJ|TRDV|TRDD|TRDJ|IGHJ|IGHV|IGKC|IGKJ|IGKV|IGLC|IGLJ|IGLV) were filtered from the variable features for subsequent ScaleData() and the RunPCA function with npcs = 50. Integration of the respective patient_timepoint datasets was achieved by using the Harmony V0.1.0 package with the following function and parameters: RunHarmony(object ,c(''orig.ident'', ''experiment_run'', max.iter.harmony =20, max.iter.cluster = 40, dims.use = 1:20, epsilon.cluster = -Inf, epsilon.harmony = -Inf). The generated Harmony reductions were used for further clustering. Hamony Dims 1:20 were used for FindClusters(..., resolution = c(0.5, 0.7, 0.9, 1.0, 1.2, 1.4, 1.5, 1.6, 1.8, 2.0)), FindNeighbors() and RunUMAP (Figures S2A and S2B).

RNA velocity analysis of the *in vitro* data

Spliced, unspliced and ambiguous expression matrices were generated for the *in vitro* datasets with the tool velocyto.py v0.17. Using the mapped annotations of cell types, all cell types annotated as $CD8^+$ were included in the analysis. For quality control, only genes with a detected exonic and intronic read in a minimum of 5 cells were selected for downstream analysis. Based on this subset, consisting of 13,893 cells, single cell momentums and velocities were calculated with pp.moments and tl.velocity using the generalized dynamical model as implemented in the package scVelo v0.2.4. A UMAP was generated for this subset of cells retaining previously defined clusters. The stream of velocities was plotted onto the embedding using the function pl.velocity_embedding_stream. A transition matrix of T-cell clusters was calculated using the methods implemented in cellrank v1.5.1. A pseudotime estimation was based on a CytoTRACE kernel, which enabled the analysis of cellular hierarchies. Macrostates were inferred using a transition matrix based on a velocity kernel and a connectivity kernel. Initial and terminal states were defined using the GPCCA-based workflow. The fate probabilities for all states were calculated for cells and driver genes were identified. These states and the fate probabilities of all cells in the clusters were visualized using directed partition-based graph abstraction (PAGA) implemented in cellrank as the function tl.paga. Finally, a circular embedding was generated using the function pl.circular_projection.

Individual clonotype dynamics

The *in vivo* VDJ .seq data for each patient was used to link the CTaa status to single cell data and annotate clonotype abundance. Shared clonotypes between the timepoints were paired and independent as well as paired clonotypes were analyzed. First, the relative abundance of each clonotype was assessed and we accounted for differences in captured clones in each timepoint by binomial sampling. The fold change for each clonotype size was then calculated. We then applied a bootstrapping-based approach, sampling 1000 times from each combined dataset per patient, stratified for cell number found in each timepoint, to calculate an empirical confidence interval for the clonotype frequency and fold change between the two captured timepoints. The bootstrapping analysis was implemented in R using the tidymodels suite of packages and the bootstraps function from the rsample package. By calculating an empirical distribution function (eCDF) for clonotype change for each patient, each individual clonotype change was categorized based on a clonal dynamic stronger than 80% of the overall clonal dynamics. Clones with a frequency above 1% before or after TCE were defined as large. Relevant expansions or contractions of a clone in each patient were calculated using the bootstrapping-based eCDF. If a clone was above or below the eCDF-based threshold in more than 95% of cases of the bootstrapping, the null hypothesis was rejected, thus the clone was defined as having undergone a significant change in clonality. To control for multiple hypothesis testing, we corrected all calculated p-values using the Benjamini-Hochberg procedure, which adjusts p-values based on the number of tests being performed in each patient sample to control the FDR. After grouping clones based on their significant clonal dynamic, universal patterns across patients were revealed by phenotype association. The association of phenotype with clonal dynamic was performed based on a majority vote of transcriptionally defined cluster associations for all cells making up each identified T cell clone. Expanding and contracting clones were then summarized for all found T cell subtypes and enrichment was tested between patients using the downstream statistical methods as outlined in the respective figure legends.

Reference-based mapping of CAR-T cell-treated patient data to *in vivo* dataset and analysis

CAR-T datasets were preprocessed consistent to *in vivo* datasets according to the steps described above. Mapping of the individual query CAR-T cell-treated patient datasets onto the TCE *in vivo* reference was done using the symphony package V.0.1.0 following the published vignette, using the log-normalisation approach: https://github.com/immunogenomics/symphony/blob/main/vignettes/Seurat.ipynb Default settings were used for mapQuery(), buildReferenceFromSeurat() and knnPredict.Seurat(). The reference Seurat object was constructed from the *in vivo* patient datasets using the same parameters as used in the initial analysis described above.

Module scores of T cell dysfunction and cytotoxicity (derived from Li et al., Cell 2019)

T cell dysfunction score

"LAG3","HAVCR2","PDCD1","PTMS","FAM3C","IFNG","AKAP5","CD7","PHLDA1","ENTPD1","SNAP47","TNS3","CXCL13","RDH10","DGKH","KIR2DL4","LYST","MIR155","RAB27A","CSF1","CTLA4","TNFRSF9","CD27","CCL3","ITGAE","PAG1","TNFRSF1B","GALNT1","GBP2","MYO7A"

T cell cytotoxicity score

"FGFBP2","CX3CR1","FCGR3A","S1PR5","PLAC8","FGR","C1orf21","SPON2","CD300A","TGFBR3","PLEK","S1PR1","EFHD2","KLRF1","FAM65B","C1orf162","STK38","SORL1","FCRL6","TRDC","EMP3","CCND3","KLRB1","SAMD3","ARL4C","IL7R","GNLY"

Cell-cell interaction analysis of human bone marrow-associated immune cells

CellPhoneDB v2.1.7 was used with the default parameters. Gene symbols were converted to ENSEMBL IDs using the clusterProfiler R package v4.0.526. CellPhoneDB analysis and visualization was run from the command line using default settings. The extraction of relevant celltype interactions and genes was achieved using the tidyverse v1.3.1 R package collection in R v4.1.0. In order to quantify the association between a given timepoint and the expression of ligand and receptor genes we utilized a random forest classifier. For improved robustness, cross-validation with 10 folds was used. The resulting model was optimized for robustness using the caret package in R.

Deep TCRB sequencing

Genomic DNA was isolated from peripheral blood samples using QIAamp DNA isolation kit (QIAGEN) as per the manufacturer's instructions. TCR beta chain (TCRB) deep sequencing was performed on purified DNA from isolated bone marrow or blood mononuclear cells to detect rearranged TCRβ gene sequences using hsTCRB Kit (Adaptive Biotechnologies) according to the manufacturer's protocol. The prepared library was sequenced on an Illumina MiSeq by the Genomics & Proteomics Core Facility, German Cancer Research Center (DKFZ). Data processing (demultiplexing, trimming, gene mapping) was done using the Adaptive Biotechnologies proprietary platform as previously described (Platten et al., 2021). ImmunoSEQ data were exported, supplemented with metadata and analyzed with R using the immunarch 0.7.0 package infrastructure. Repertoire overlap was calculated using Morisita's or Jaccard overlap indices. Estimation of repertoire diversity was performed using the repDiversity function. Longitudinal clonotype tracing was calculated with the trackClonotypes function.

Functional TCE testing in *in vitro* bone marrow cultures

Primary human co-cultures

Bone marrow mononuclear cells were isolated as described above. CD138+ cells (live/CD45-/CD138+) and $CD3^+$ (live/CD45+/CD3+) cells were isolated by fluorescence-activated cell sorting (FACS) on a BD FACSAria™ Fusion cell sorter. Malignant plasma cells and T cells were counted and co-cultured at a 1:1 ratio in ImmunoCult-XF T Cell Expansion Medium (STEMCELL technologies) supplemented with 50 IU/ml recombinant human IL-2, 25 ng/ml IL-7 and 25ng/ml IL-15. From each well, 10.000 T cells were sampled for scRNA/VDJ-seq as described above to generate T_0 data. Plasma cells were verified to express BCMA by flow cytometry. A recombinant anti-BCMA x anti-CD3 CrossMab bispecific antibody was used to stimulate T cell activation by malignant plasma cells. To assess HLA class I dependency of observed T cell reactivity, co-cultures were incubated with anti-HLA class I antibody (W6/32). To detect T cell clones reactive against common viral epitopes, T cell only cultures were incubated with CEFT pool, 120nmol >70% (JPT Peptide Technologies). Every 3 days, fresh medium with 50 IU/ml recombinant human IL-2, 25 ng/ml IL-7 and 25ng/ml IL-15 was added to the culture. After 7 days of co-culture, all cells were counted, collected by centrifugation at 500g for 5min and lysed in DNA lysis buffer and genomic DNA was isolated using QIAamp DNA isolation kit (QIAGEN) as per the manufacturer's instructions. Deep VDJ-seq was performed as described above to generate T_7 data.

Reference-based mapping of *in vitro* data to *in vivo* dataset and analysis

In vitro datasets (T_o) were preprocessed consistent to *in vivo* datasets according to the steps described above. Mapping of the individual query *in vitro* single cell datasets onto the *in vivo* reference was done using the symphony package V.0.1.0 following the published vignette, using the log-normalisation approach: https://github.com/immunogenomics/symphony/blob/main/vignettes/Seurat.ipynb Default settings were used for mapQuery(), buildReferenceFromSeurat() and knnPredict.Seurat(). The reference Seurat object was constructed from the *in vivo* patient datasets using the same parameters as used in the initial analysis described above. TCR overlap analysis between single cell and bulk TCRseq datasets was performed using the R Version 4.0.0 environment especially using the dplyr package V.1.0.7. Clonotype overlap was identified by the amino acid sequence of the respective CDR3 region. For

deep VDJ-seq and single-cell VDJ-seq comparisons only the TCR beta chain was used. Only TCR clones successfully detected and mapped in both *in vitro* datasets (T_0 scRNA/VDJ-seq and T_7 deep VDJ-seq) were used in downstream analysis.

Data visualization

Tabular data from single-cell sequencing analyses above were processed using the tidyverse suite of packages [https://CRAN.R-project.org/package=tidyverse] and visualized in the R programming environment using the ggplot2 package. Data from all other analyses were visualized using GraphPad Prism 9.0. Figures were produced using Adobe Illustrator 2022. Graphical Abstract was created with BioRender.com. Density Plots were generated using the scRepertoire package V.1.3.1 using the getCirclize(..., cloneCall = "CTaa", groupBy = "timepoint", proportion = FALSE) and clonalOverlay(freq.cutpoint = 0.01, bins = 25,...) functions. The top TCRs were selected based on the relative frequencies for each clonotype calculated by the scRepertoire package. DotPlots were subsequently created using the ggplot2, tidyverse and dplyr packages.

QUANTIFICATION AND STATISTICAL ANALYSIS

Data are represented as individual values or as mean ± SEM, as indicated. Group sizes (n) and applied statistical tests are indicated in figure legends. Significance was assessed by either unpaired *t*-test analysis, paired *t*-test analysis, or two-way ANOVA analysis with multiple hypothesis testing correction as indicated in figure legends. All reported p values are two-tailed. All analyses were performed using either R v4.1.0 (www.R-project.org) and Bioconductor v3.4 or GraphPad Prism 9.0.

Due to the nature of this study, sample size determination was not applicable, as all available samples were included in this study. All cells passing QC (Figures S1 and S2 and Table S2) were included in downstream analyses on a single-cell basis. For functional experiments, bone marrow samples were blinded to the experiment performers.